MODULATION AND SAMPLING OF HYDROMAGNETIC RADIATION*

C. P. Sonett

National Aeronautics and Space Administration
Space Sciences Division
Ames Research Center
Moffett Field, California

29415

act: It is shown that detecting electromagnetic signals
in the hydromagnetic domain by means of magnetometers is
a low frequency extension of the electromagnetic spectrum;
therefore conventional modulation theory is employable,
subject to the special constraint that the carrier fre-
quency is determined by spacecraft motions. In the pres-
ence of a hydromagnetic continuum, spacecraft spin
modulation folds the spectrum so that fictitious offsets,
ambient field errors, and the generation of spurious wave
signals can occur, the latter from single sidebanding.
Synchronous demodulation by means of time quadrature
detectors can be employed to remove such effects. Com-
mutated telemetry which time shares experiments is shown
to yield a multirate sampled spectrum. This telemetry
can cause uncorrectable spectral folding of many orders
because it generates a complex switching spectrum con-
taining a subsidiary multiplet structure about each of
the principal switching tones.

---

*To be presented at the COSPAR-URSI Symposium on Optimi-
zation of Instrumentation for Space Experiments from the Stand-
point of Data Processing, Buenos Aires, May 1965.

TMX - 56428

1. Introduction

The magnetospheric and interplanetary plasmas are regarded as fluids to which is coupled an ambient magnetic field with an electromagnetic radiation field completing the ensemble. The spectral content is determined locally both by plasma kinetics and the form of the source which drives the time varying field, except when local plasma instabilities are important, or the decay of turbulent motions is dominant. The rapid flow of the interplanetary plasma against a spacecraft means that all frequencies are Doppler shifted and time versus space variations cannot be simply distinguished. Thus the time reversibility of propagating waves becomes mixed with the diffusion-like and irreversible decay of large spatial disturbances into smaller ones, the familiar cascading from small to large wave numbers in turbulence.

Of special interest is the low frequency region of the spectrum associated with hydromagnetic radiation, as both wave and convective frequencies of the solar gas encompass characteristic frequencies of motion of spacecraft. It ensues that certain modulation effects take place which can modify the interpretation of signals from the field. The modulation has a geometric basis which in principle generalizes to any detector in motion. Spacecraft rotation has an especially simple modulation effect upon magnetic signals which can be explained by an extension of existing modulation theory. The special quality of the modulation arising from spacecraft spin is due to the

superposition of similar frequencies from the radiation field and the spacecraft. This situation favors the development of asymmetric and truncated side band spectra which in turn can "alias" the signal.* Variations of the discussion of this paper can be extended, for example, to particle detectors following the arguments laid down here.

The plan of the paper is to consider first what happens when a magnetic field in space is measured by a magnetometer mounted upon a spacecraft which is executing motions about its center of gravity. Specifically, the magnetometer will be assumed to decompose the field into three orthogonal components as is the case for the triaxial flux gate. The spacecraft will be assumed to spin about the figure axis, as this analysis provides a realistic view of the resultant modulation process. Both the changes in amplitude and changes in direction of the field are examined separately, and the general case of both types of time dependence occurring simultaneously will be shown to be a simple combination of these two. For instruments which measure the field directly, in contrast, say, to search coils which operate upon the field by time differentiation, the two

---

*The term alias is jargon used to denote first order folding of spectra due to violation of the Nyquist limit in the sampling of continuous data. This special case, discussed later in the text (see fig. 11), is used interchangeably in this paper with spectral shifting which is a generalization of first-order spectral folding.

distinct types of field variation generate, respectively, amplitude and phase modulation of the output signal from the spacecraft. For a nonrotating spacecraft platform, the former degenerates to the trivial case of AM modulation with zero carrier frequency whereas directional changes in the field generate more complex signals. For brevity these two effects are termed scalar and vector modulation, respectively, recognizing that the latter term is not exact. This discussion is followed by a discussion of the search coil on a spinning spacecraft. The signal properties are shown to be different according to the operation of time differentiation inherent in this type of detector. Following this, attention is directed to the correspondence of data multiplexing (customarily employed in single channel spacecraft telemetry) to multirate switching and the spectral overlap or alias problem. Lastly, the application of synchronous demodulation to spin modulated signals is considered. Synchronous detection employing quadrature signals provides a means for the electrical despinning essential for the unfolding of side band structure.

In the discussion that follows it is always assumed that the system response is linear, so that harmonic generation from this source is absent. Thus the arguments entail only modulation of a linear system, and spectral folding and shifting from multi-periodic sampling as occurs in time shared telemetry. Also arguments regarding spacecraft motions which involve precession and nutation are not considered, having been discussed elsewhere [1,2].

2.0 Convection and Radiation

It is thought that in the solar wind, spatial structures of nearly any size should be allowed and the gyro radius is not an essential limit, though the more time stationary and organized forms such as shocks and contact discontinuities should display a limit more or less corresponding to the ion gyro radius. Since the wind is in motion with a proper velocity of some hundreds of kilometers per second, it is clear that such a limit means that to observe the details of diffusion of a contact discontinuity or other similar organized change in the gas and the field requires that a magnetometer have a frequency response of at least 1 cps or more. There are other phenomena in the interplanetary gas which are presently little understood such as the alternating polarity of tubes of force emanating from the sun. How these merge where opposed polarities meet has at least superficial similarity to questions relating to contact discontinuities.

Although propagating waves are, in practice today, indistinguishable from spatial changes in the solar wind, in the magnetosphere bulk velocities should be much reduced and perhaps absent from time to time, though there is no empirical basis for assuming this. In either case when the field is sufficiently steady and large to form a reference frame for waves, the geometry rules governing plasma waves should be applicable to convected disturbances.

Only a simplified view of wave phenomena is required for the ensuing arguments as they will rest partially upon geometry.

Consideration of the allowed wave modes is restricted to the
hydromagnetic domain governed primarily by ion motions. Exten-
sion upwards implies inclusion of frequencies not properly the
province of hydromagnetics. From geometrical considerations
alone the three governing modes become the Alfvén shear wave
and the two mixed waves representing fast and slow modes. These
have phase velocities which depend both upon the Alfvén and sonic
speeds. The corresponding surfaces of constant phase are shown
in fig. 1. It is seen that propagation across the field is
allowed only for the fast mode while along the field direction
two waves can propagate. The diagram is the zero frequency
limit and displays no dispersion. (In a broader sense, however,
there is a functional relation between speed of propagation and
direction with respect to the preferred axis of the field.)
The linearly polarized Alfvén mode displays rotation of the
plane of polarization as the gyro frequency of the plasma is
approached from the lower side. Above ω_g only one-handedness
persists. Thus the Alfvén wave is circularly polarized in
regions near to and above the gyro resonance. In interplane-
tary space ω_g is typically of the order of 1 cps and therefore
is important for magnetometer experiments. For the Alfvén mode
the disturbance vector is normal to the field and gyrates about
the latter, as shown in fig. 2. Propagation across the field
consists of alternate collective compression and rarefaction
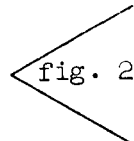in the field and the gas pressure, while for the Alfvén mode

fig. 1

fig. 2

the motion is incompressible. These two limiting conditions
form the geometrical background for the discussion of modulation
effects to follow.

Purely compressive changes in the field associated with
progressive or standing waves are subject to amplitude modula-
tion by the spinning reference system. Alfvén waves are phase
modulated by the spin. It is more convenient to invert these
problems so as to regard the spin as the carrier and the hydro-
magnetic radiation as the source of the modulation. There is
no loss of generality in doing this and the analysis, in par-
ticular, of the phase modulation is simplified considerably.

By way of summary, it is assumed that variations in the
field, both spatial and time dependent, are representable by
simple geometric constructions so that the main points discussed
are not obscured by detailed development of the allowed modes
for propagating waves in a plasma. The problem becomes one of
synthesizing the signal characteristics of magnetic field vari-
ations from data taken in a hydromagnetic radiation field hav-
ing spectral components which beat with the spin frequency of
the spacecraft. Since spatial variations are not separable
without recourse to other data, especially plasma probe infor-
mation, for the purposes of this discussion they will be treated
as strictly time variant. Further we shall assume that the
hydromagnetic field consists of a continuum of frequencies, and
only for the purposes of illustration will deviation be made
from this choice.

The compressive case corresponds to the rms sum of the Alfvén and the sonic speeds taken across the preferred direction of the field. This is the most straightforward case to treat as the field suffers only changes in amplitude and thus the magnetic signal consists of beats between the spin and the hydromagnetic spectrum. The preferred direction of the magnetic field is generally not along the spin axis of the spacecraft; thus the field is resolved into spacecraft coordinates.

3.0 The Scalar Hydromagnetic Radiation Field and Spectral Folding

The simplest radiation field to treat is that corresponding to the magnetic field undergoing compressive changes associated with fast wave propagation across the field lines. This simple time variance is now considered with the signal detected upon a spinning spacecraft, and it will be shown that a spectral line splits in a manner strictly analogous to amplitude modulation where the spin frequency of the spacecraft assumes the role of the carrier.

Since the field static direction is assumed known, as is that of the spacecraft, the components of the field are resolved into spacecraft coordinates directly. Let $(\vec{x}_1, \vec{x}_2, \vec{x}_3)$ be a right-handed, mutually orthogonal set of unit vectors associated with the ambient field passing through the spacecraft position with $\vec{x}_1$ along the line of force taken positive in the direction of the field, $\vec{x}_2$ the unit vector lying in the magnetic meridian plane and having positive sense outward (for the interplanetary field where a preferred direction is more difficult to define

other appropriate coordinates such as solar ecliptic are available), and $\vec{x}_3$ the unit binormal to the field line. The notation $(\hat{x}_1, \hat{x}_2, \hat{x}_3)$ is given to a second set of unit vectors centered in the spacecraft but nonrotating. The spin axis of the vehicle is given by $\vec{\omega}_S = |\omega_S|\hat{x}_3$ which defines the direction of the unit vector, $\hat{x}_3$. It remains to define the line of nodes between the two sets of vectors to complete the description.* The orientation of the spacecraft with respect to the magnetic field is then given by the two Eulerian angles, θ and φ. The third angle, ψ, the rotation about the axis, x_3, is arbitrary and taken to be zero. The nominal or ambient magnetic field is given by $\vec{H}_0 = |H_0|\vec{x}_1$. To this must be added the perturbation field which is represented by the Fourier transform pair

$$H(t) = (1/\sqrt{2\pi}) \int_{-\infty}^{\infty} h(\omega)\exp(i\omega t)d\omega \tag{1}$$

$$H(\omega) = (1/\sqrt{2\pi}) \int_{-\infty}^{\infty} H(t)\exp(-i\omega t)dt \tag{2}$$

where $H(t)$ is the disturbance waveform and $h(\omega)$ is the spectral density of the field disturbance in units of field intensity per radian per second. For the case at hand where the field variations are taken to be strictly compressive, the variation field is in the direction $\vec{x}_1$. Thus the total field is given by

$$\left.\begin{array}{l} H_1 = H_0 + H(t) \\ H_2 = 0 \\ H_3 = 0 \end{array}\right\} \tag{3}$$

---

*The Euler angle definitions used follow those of Goldstein [3].

In the nonrotating, spacecraft centered coordinate system $(\hat{x}_1, \hat{x}_2, \hat{x}_2)$, the components of the field are resolved into

$$_\wedge H_1 = H_1 \cos \varphi + H_2 \sin \varphi \tag{4a}$$

$$_\wedge H_2 = -H_1 \sin \varphi \cos \theta + H_2 \cos \varphi \cos \theta + H_3 \sin \theta \tag{4b}$$

$$_\wedge H_3 = H_1 \sin \varphi \sin \theta - H_2 \cos \varphi \sin \theta + H_3 \cos \theta \tag{4c}$$

The angles θ and φ are taken to be fixed for times comparable to those of interest. Thus in turn $_\wedge H_2$ and $_\wedge H_3$ may be regarded as fixed.

3.1 The Generation of AM Side Bands

Consider now a triaxial set of sensors, such as flux gates mounted upon a spacecraft having spin angular velocity ω_s. The sensors lie, respectively, along the spin axis, $\hat{x}_3$, and mutually orthogonal in the equatorial plane. Let $\hat{c}_1$ and $\hat{c}_2$ be the unit vectors associated with the two equatorial sensors. The time origin is chosen so that $\hat{c} = \hat{c}_1 \cos(\omega_s t) + \hat{c}_2 \sin(\omega_s t)$. Then the components of the field as observed from the rotating platform of the spacecraft are given by $(\hat{\vec{H}} \cdot \hat{c})$ or

$$_\wedge H_1 \cos(\omega_s t) \tag{5a}$$

$$_\wedge H_2 \sin(\omega_s t) \tag{5b}$$

where the phase is arbitrarily adjusted so $\hat{\vec{H}} = {}_\wedge H_1$ at $t = 0$. For algebraic simplicity, the spin tone is collapsed to a delta function and convolution of the spin tone with the hydromagnetic field yields a total spectral density distribution given by

$$H_0 \delta(\omega_s) + (1/2)h(\omega)[\delta(\omega_s + \omega) + \delta(\omega_s - \omega)] \tag{6}$$

which means that the spin tone beats with the hydromagnetic spectrum corresponding to direct amplitude modulation. The special quality is associated with the embedding of the spin tone or carrier frequency in the frequency domain of the hydromagnetic radiation field. The second two terms in eq. (6) together with the carrier can be represented in the conventional manner as spinning vectors as shown in fig. 3. In the inertial frame the two vectors rotate with angular velocities $\omega_S + \omega$ and $\omega_S - \omega$. In the frame which transforms away $\bar{\bar{H}}_O$, they rotate with velocities ω and $-\omega$. This is an important effect for the situation discussed in the next section.

fig. 3

Contributions to $h(\omega)$ neighboring ω_S are translated to regions near the origin while those near the origin translate to the neighborhood of ω_S. Alternatively on a frequency plot showing negative frequencies, side band symmetry about ω_S would extend the spectrum to negative frequencies. The mixing of the hydromagnetic spectrum with the spin tone splits the power shown in the side band structure according to eq. (6) where half the power from a band $\Delta\omega$ is shifted into each of the side band components. The overlapping of translated side bands, however, does not allow a direct computation of the power in a particular region of the spectrum unless the functional form of $h(\omega)$ is given.

When the frequency band lies in the interval $0 < \Delta\omega < \omega_S$ the upper side band is found at $\omega > \omega_S$. For frequencies in the

interval $\omega_s < \Delta\omega < 2\omega_s$, reflection about zero frequency occurs

so that the lower side band is still contained in the interval

$0 < \Delta h < \omega_s$ with the spectral form inverted. However, for

those regions of the frequency domain of $h(\omega)$ which lie above

$2\omega_s$, the modulation process generates both side bands asymmetri-

cally above the carrier. This is a direct result of the low

carrier frequency and is never found in normal communication

practice [4] where the modulation is bounded to a small frac-

tion of the carrier frequency (see fig. 4).

3.2 Single Side Band Generation of Pseudo-Alfvén Signals

Consider a real system where the upper frequency limit is

defined by a filter that is flat out to ω_c where $\omega_c > \omega_s$

and rolls off beyond ω_c at some preassigned rate. Then all

frequencies below $\omega^* < \omega_c - \omega_s$ will be recovered without

spurious information. For those contributions to $h(\omega)$ where

$\omega^* \geq \omega_c - \omega_s$, the upper and lower side bands will display

different amplitudes according to the expression

$$H_o\delta(\omega_s) + (1/2)h(\omega)[a\delta(\omega_s - \omega) + b\delta(\omega_s + \omega)] \qquad (7)$$

where a is unity for modulation frequencies, $\omega < \omega_s + \omega_c$,

b is unity for $\omega < \omega_c - \omega_s$, and $h(\omega)$ is the spectral density

when $\omega < \omega_c$. When $h(\omega)$ lies in the range of the slope of the

filter, then it must also be replaced by an equivalent $h^*(\omega)$

since the modulation tone is attenuated. From eq. (7) it is

seen that the side band components are attenuated by different

amounts since they lie at different points on the filter ramp.

Reference to fig. 5a shows an idealization of the above.

fig. 4

fig. 5a

An important effect of the truncation of the side band structure is to introduce a spurious phase modulation whose most general interpretation suggests the presence of Alfvén waves when none are present in the field. This is seen by reference to fig. 5b where a vectorial representation of the pertinent signals shows the manner of composition of the total signal. When the side band structure is symmetric, it is seen that the two side bands are symmetrically disposed about the carrier vector, with the result that phase contributions are cancelled.

fig. 5b

The case of the line spectrum shown in fig. 5 has the equivalent time expression (see fig. 6)

fig. 6

$$H_0 \cos \omega_s t + \frac{(a+b)}{2} (\cos \omega_s t \cdot \cos \omega_t) + \frac{(a-b)}{2} (\sin \omega_s t \cdot \sin \omega_t)$$

(8)

and the quadrature side bands are in ratio $(a + b)/(a - b)$. When the upper side band is suppressed completely, the in-phase and quadrature components are equal and the power in the sinusoidal and cosinusoidal parts of the carrier are equal. This means that only in the event the value of $h(\omega)$ drops to zero for all $\omega > \omega_c - \omega_s$ can it be guaranteed that a spurious Alfvén wave field will not be introduced. The results of this section can be summarized as follows:

In the presence of a scalar hydromagnetic radiation field, that is, containing only waves characterized by changes in field amplitude, the signal from a magnetometer sensor which

measures the instantaneous field normal to the spin axis of a
rotating spacecraft having a spin frequency, ω_S, will contain
both in-phase and quadrature modulation side bands derived from
that portion of the radiation spectrum lying at frequencies in
the range $\omega_C - \omega_S < \omega < \omega_C + \omega_S$ where ω_C is the filter break
frequency of the system.

3.3 Spacecraft Pseudo-Perm and Ambient Field Offset

Consider now that portion of the hydromagnetic spectrum,
$h(\omega)$, that overlaps the spin frequency, ω_S. Because of modula-
tion, this portion of the spectrum is folded to the neighborhood
of $\omega = 0$; consequently a pseudo-bias appears in the spin signal
as perceived at the receiver. Depending upon the time of averag-
ing, which determines the line width at zero frequency, an error
could be introduced into the measurement of the offset which,
in turn, measures the component of the spacecraft bias lying in
the equatorial plane of the spacecraft. Although in practice
this offset of the magnetometer signal may be undetectable, it
is important to point out that in principal it is always present.
Its value will depend, as stated above, upon the filter band-
width used to assess the offset and the power in the hydromag-
netic spectrum about the spin frequency.

The arguments just given can be applied in a broader context.
For example, if the hydromagnetic field contains frequencies
which are dominant at twice the spin frequency, the folding of
these with the spin frequency will cause them to appear as addi-
tions to the basic sinusoidal signal. Customarily this signal

is interpreted as arising solely from the static component of
the magnetic field which is projected into the equatorial plane
of the spacecraft. Then the measurement of the static field will
be increased by some amount determined by the power in the hydro-
magnetic domain nearly twice the spin frequency and the length
of the sampling interval used to measure the spin tone, or,
equivalently, the filter bandwidth.

In arguing the importance of these folded contributions to
the measurement of the static field and the spacecraft perm, it
is clearly important to understand the form of the spectral com-
ponents involved in the process. To a point, common sense must
be applied in studying data of the type discussed. However,
cases can be expected to arise where, in spite of the natural
appearance of the data, it does happen that important folding
from the modulation takes place; such cases cannot be distin-
guished from the unfolded data by any a posteriori means.

3.4 The Aperiodic Field Reversal

Occasions arise especially in the interplanetary field
when a reversal in polarity takes place over a time interval of
the order of five minutes by present best estimate [5,6].
Actually the time interval may be considerably shorter; it is
also important to recognize the role of convection in this
description since the field is being swept past the magnetom-
eter. Thus the change of field may be primarily spatial, but
in the coordinate system of the magnetometer, can be considered
to be strictly a time variation. Interest stems as before in

the role played by folding of the spectral components of the field change with the spin tone from a rotating sensor. A quantitative treatment is beyond the scope of this paper; however, the simple field discontinuity can be represented by a step function; it is recognized that more complicated field changes can take place involving skewing, with the field never reaching zero magnitude. Such changes are also outside the province of this discussion as they involve rotation of the magnetic vector corresponding to phase modulation discussed in the next section.

The Fourier transform of the step function is of the form $1/\omega$ and is unbounded near the origin. Thus when folded onto the spin frequency, the net spectrum takes on the character displayed in fig. 7 which shows the low frequencies shifted to the spin tone. The regions near zero frequency are not especially interesting from a physical standpoint as they correspond to the tails of the function where the value is steady. Of principal interest are the higher frequencies which provide information on the thinness of the discontinuity and on fluctuations. In spite of the divergence of the transform around the spin frequency as shown in fig. 7, the power must correspond to the steady-state field far from the discontinuity. There is considerable spectral energy near zero frequency which, correctly interpreted, should correspond to regions of the step spectrum near the spin frequency. Lastly, there is a strong increment of the spectrum which is shifted to higher frequencies.
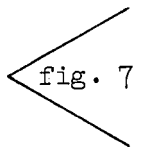
fig. 7

The general effect of these folding phenomena is to decrease the apparent thickness of the region of transition, to possibly introduce a pulse-like change in the spin tone and, lastly, to introduce an aperiodic transient change of the zero or average level of the magnetometer signal.

4.0 Vector Modulation

In this section the signal resulting from the detection of the propagating Alfvén mode is considered. The geometry of the wave in the previous coordinate system $(\vec{x}_1, \vec{x}_2, \vec{x}_3)$ will be the basic reference for the following discussion. We assume that the mode is linearly polarized but that the plane of polarization turns slowly subject to an ion Faraday rotation. Near the gyro resonance for protons, one of the modes is extinguished and the wave is regarded as circularly polarized with a gyration period equal to the Larmor period. Since the ambient field has a fixed orientation, the resolution of the wave into components of the prescribed set follows directly the rules for phase modulation with suppressed carrier. Thus the field components are given by

$$\left. \begin{aligned} H_1 &= H_0 \cos \xi \sin(\delta \sin \nu t) \\ H_2 &= H_0 \sin \xi \sin(\delta \sin \nu t) \\ H_3 &= H_0 \cos(\delta \sin \nu t) \end{aligned} \right\} \qquad (9)$$

where ξ is the dihedral angle between the instantaneous plane containing the wave and the plane $\vec{x}_1\vec{x}_3$. The other quantities are defined as follows: ν is the frequency of the Alfvén wave

assumed monochromatic, and δ is the deviation in phase corresponding to the angular deviation of the quiescent field around its nominal orientation. From eqs. (9) it is clear that the geometrical resolution of the time-dependent field directly generates phase modulated signals in each of the sensors. In general, the spacecraft will not have a preferred direction and therefore the components of eqs. (9) must be resolved through an Eulerian transformation. In the new set $(\hat{x}_1, \hat{x}_2, \hat{x}_3)$ defined as in the previous section centered in the spacecraft, the field is given by

$$\hat{\vec{H}} = [T]\vec{H} \tag{10}$$

where $[T]$ is the Eulerian rotation matrix. In the most general instance the spacecraft is allowed to rotate about its axis of symmetry with $\psi = \omega_s t$. More general motions described as tumbling where all the Eulerian angles become time dependent are not considered. In the instance of spin the process of signal modulation enters as in the earlier discussion of amplitude effects though in a more complex way. Even the resolution into components itself is important in mixing the modulation components. The components of the field under phase modulation of deviation, δ, at frequency, ν, are expressed for a general orientation by

$_{\wedge}H_1 = H_0[a_{11} \cos \xi \sin(\delta \sin \nu t)$

$\qquad + a_{12} \sin \xi \sin(\delta \sin \nu t) + a_{13} \cos(\delta \sin \nu t)] \tag{11a}$

$$_\wedge H_2 = H_0[a_{21} \cos \xi \sin(\delta \sin \nu t)$$

$$+ a_{22} \sin \xi \sin(\delta \sin \nu t) + a_{23} \cos(\delta \sin \nu t)] \qquad (11b)$$

$$_\wedge H_3 = H_0[a_{31} \cos \xi \sin(\delta \sin \nu t)$$

$$+ a_{32} \sin \xi \sin(\delta \sin \nu t) + a_{33} \cos(\delta \sin \nu t)] \qquad (11c)$$

where $_\wedge H_1$, $_\wedge H_2$, and $_\wedge H_3$ are the components of the field in the $\wedge$ system, and the a_{ij} are the elements of the matrix, given in eq. (10).

It is to be noted that linear mixing of the various side band tone systems depends on both the orientation of the plane of polarization of the wave and the orientation of the spacecraft as reflected in the elements of the transformation matrix, a_{ij}. The terms in eqs. (11) are recognized as the usual expressions encountered in phase modulation. The carrier is suppressed and $_\wedge H_1$, $_\wedge H_2$, and $_\wedge H_3$ contribute combinations of odd and even harmonics. The amplitudes of the side band tones are given by Bessel functions of the first kind, utilizing the following expansions:

$$\sin(\delta \sin \nu t) = 2 \sum_{n=-\infty}^{\infty} J_{2n+1}(\delta)\sin(2n + 1)\nu t \qquad (12a)$$

$$\cos(\delta \sin \nu t) = J_0(\delta) + 2 \sum_{n=-\infty}^{\infty} J_{2n}(\delta)\cos 2n\nu t \qquad (12b)$$

When these are inserted in eqs. (11) it is recognized that for the most general orientation of the spacecraft, each of the component

magnetometers measures a spectral complex consisting of linear combinations of odd and even terms with corresponding Bessel function amplitudes. The spectrum of each of the expressions given above is shown in fig. 8 for the case chosen of a maximum phase deviation of 1.5 radians corresponding to a large Alfvén wave which causes an instantaneous variation in field direction of $\sim\pi/2$.* Also it is assumed in this figure that a wave train exists with a single frequency given by ν. The number of significant side bands depends only upon the phase deviation and therefore the total bandwidth encompassed varies directly with the phase excursion frequency; that is, the separation between side bands varies with ν. Since the modulation is about zero frequency, i.e., the static field, the field aligned spectral components are even functions; fig. 8 represents terms which when folded add to double value in the positive frequency domain. When the power spectra are considered, only the positive frequency domain is present. The components from the negative domain are folded about zero frequency. Mathematically this follows from the odd and even order Bessel functions being of odd and even symmetry, respectively. Thus in eqs. (12a) and (12b) the expressions are seen to be even for each case.

fig. 8

---

*In all expansions discussed in this section the frequency domain is taken over $-\infty \leq \omega \leq \infty$ for reasons of symmetry. The practical case of measurement discussed in section 7 reverts to folding about $\omega = 0$ since laboratory frequency analysis precludes $\omega < 0$.

In the event that sufficient power is available in the side band structure for detailed analysis it becomes evident that field orientation information can be derived from the relative amplitudes of the even and odd side bands. These determine the orientation of the figure axis of the spacecraft with the direction of the ambient field. Regarding the suppressed carrier condition, it is seen by examination of eq. (12a) that since the signal spectrum is expanded about zero frequency, the carrier is nonexistent for the odd harmonic series. However, carrier suppression for the even series can also occur when the field is deviated by 2.4 radians which is the first root for J_O. Zeros for the higher order functions would be physically unreal and are therefore not discussed. Even deviations of 2.4 radians seem unlikely for a physically real Alfvén wave as the field would have to be folded over on itself.* We now write the complete expressions for the field components for the three axes for arbitrary orientation of the spacecraft. From eqs. (11) and (12) they are

$$_\wedge H_1 = H_O \left\{ \left[(a_{11} \cos \xi + a_{12} \sin \xi) \times 2 \sum_{n=-\infty}^{\infty} J_{2n+1}(\delta) \sin(2n+1)\nu t \right] \right.$$

$$\left. + a_{13} \left[J_O(\delta) + 2 \sum_{n=-\infty}^{\infty} J_{2n}(\delta) \cos 2n\nu t \right] \right\} \qquad (13a)$$

*The restriction in angular deviation would not necessarily hold for the case where aperiodic changes in direction of the field occurs as where tubes of opposed polarity swept across the spacecraft.

$$\wedge H_2 = H_0 \left\{ (a_{21} \cos \xi + a_{22} \sin \xi) \times 2 \sum_{n=-\infty}^{\infty} J_{2n+1}(\delta) \sin(2n+1)\, \nu t \right.$$

$$\left. + a_{23} \left[J_0(\delta) + 2 \sum_{n=-\infty}^{\infty} J_{2n}(\delta) \cos 2n\nu t \right] \right\} \tag{13b}$$

$$\wedge H_3 = H_0 \left\{ (a_{31} \cos \xi + a_{32} \sin \xi) \times 2 \sum_{n=-\infty}^{\infty} J_{2n+1}(\delta) \sin(2n+1)\, \nu t \right.$$

$$\left. + a_{33} \left[J_0(\delta) + 2 \sum_{n=-\infty}^{\infty} J_{2n}(\delta) \cos 2n\nu t \right] \right\} \tag{13c}$$

These are the most general expressions for pure Alfvén wave modulation. Below about 0.3 radian deviation the side band structure collapses to two lines given by the terms J_1. Thus for small amplitude Alfvén waves the modulation spectrum is barely distinguishable from that produced by simple scalar modulation of the field. The separation of the side bands is still given by the modulating frequency. The even order series of terms vanishes and the scheme becomes especially simple. The only feature distinguishable from the scalar modulation is that the upper and lower side bands are in phase opposition, and modulation represented by the even series vanishes.

It is anticipated from the foregoing discussion that the internal bandwidth requirement for nontruncated detection of vector modulation can be greater than for the scalar case when the modulating frequencies are identical.

The guiding parameter is the total excursion in phase of the Alfvén wave which, in the language of modulation theory, is the phase deviation. As the modulation frequency is increased, the side band structure will expand over the frequency domain but the number of relevant side bands is uniquely determined by the phase deviation. It is not expected that for Alfvén waves that this will ever exceed three side bands.

The situation is more complex when tubes of force which have skewed or opposed polarities sweep across the magnetometer. For, in this instance, the instrument sees a time rate of change whose spectrum is to be represented by a Fourier integral.

4.2 The Circularly Polarized Mode

This case has no essential differences from that discussed in the last section except that the time variation in ξ now becomes important enough to warrant consideration of the mixing of this tone with the spectrum from the vector modulation. Earlier the angle of the plane of polarization was assumed nearly time invariant which was taken to include slow rotation of the plane of polarization.

For simplicity it is assumed that the spacecraft is aligned with the preferred direction of the field; that is, one of the axes, say $\vec{x}_3$, corresponds to the ambient field direction. For the wave propagating above the gyro cutoff, $\dot{\xi}$ is equal to the gyro frequency for the ions under consideration, which we take here to be protons. The components of the field in the

$(\vec{x}_1, \vec{x}_2, \vec{x}_3)$ set are as in eqs. (12) with $\dot{\xi}$ periodic. The signals from the $\hat{x}_1$ and $\hat{x}_2$ sensors are in quadrature as are the components, $\vec{H}_1$ and $\vec{H}_2$. The field component along $\vec{H}_3$ is fixed and represented in eqs. (13) by collapsing all the terms to zero except J_0. From eqs. (13) it is seen that terms of the type

$$\cos \xi \, \sin(2n + 1) \nu t$$

and

$$\sin \xi \, \sin(2n + 1) \nu t$$

are generated, respectively, for the H_1 and H_2 signals. Thus $\dot{\xi}$ beats with an odd harmonic spectrum, generating additional side tones. The final side band composition is formed from the expansions of eqs. (13) and are

$$_{\wedge}H_1 = H_O \sum_{n=-\infty}^{\infty} J_{2n+1}(\delta) \times \{\sin[(2n+1)\nu + \dot{\xi}]t + \sin[(2n+1)\nu - \dot{\xi}]t\}$$

(14a)

and

$$_{\wedge}H_2 = H_O \sum_{n=-\infty}^{\infty} J_{2n+1}(\delta) \times \{\cos[(2n+1)\nu - \dot{\xi}]t - \cos[(2n+1)\nu + \dot{\xi}]t\}$$

(14b)

The $_{\wedge}H_1$ signal is composed of line pairs above and below $\dot{\xi}$, spaced at intervals of $\pm(2n + 1)\nu$ while $_{\wedge}H_2$ contains side bands of the same form but with phase in quadrature with the $_{\wedge}H_1$ terms. The meaning of these expressions is straightforward. The amplitude of the side bands is given by the J_{2n+1} terms and the side band phases oscillate in quadrature with respect to the field components along each of the axes. The two sensors

have a side band relation displaced by $\pi/2$ since when the $\vec{x}_1$ signal is peak, its rate of change is zero while that for the $\vec{x}_2$ sensor is a maximum. The vector sum of each of the side band contributions from these two sensors has constant amplitude and contains only the angular frequency $(2n + 1)\nu$. (See fig. 9.)

4.3 Modulation of the Search Coil

The apparent simplicity of the search coil as a field detector is subject to reconsideration in the presence of a hydromagnetic radiation continuum. This instrument as orig- inally used measured a projected value of the ambient field together with time variations. The ambient field could be detected as a carrier tone since the coil was used with a rotating spacecraft. Later usage has employed attitude sta- bilized craft, resulting in a simpler measurement problem.

For the spinning spacecraft, the problem of measurement of field variations is compounded by the combination of differentiation inherent in the detector together with the rotation of the spacecraft. Since this subject has been explored earlier, only the principal results will be dis- cussed here [7]. They have special interest since the dif- ferentiation process introduces an apparent phase modulation in the presence of a strictly scalar radiation field. The inverse process also takes place when the field contains only an ensemble of Alfvén waves.
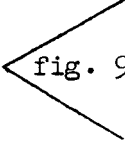
fig. 9

Utilizing the coordinate systems specified earlier, the voltage output from a search coil spinning in a field containing time dependent terms along all resolved components is given by*

$$\epsilon = -[\dot{H}_1^* \cos \varphi + \dot{H}_2^* \sin \varphi + \omega(-H_1 \cos \theta \sin \varphi + H_2^* \cos \theta \cos \varphi$$

$$+ H_3^* \sin \theta)]\cos \omega t$$

$$-[-\dot{H}_1^* \cos \theta \sin \varphi + \dot{H}_2^* \cos \theta \cos \varphi + \dot{H}_3^* \sin \theta$$

$$- \omega(H_1 \cos \varphi + H_2^* \sin \varphi)]\sin \omega t \qquad (15)$$

where the angles, φ and θ, are those defined before and H_1^*, H_2^*, and H_3^* are the components of the disturbance field which together with H_0 form the total field

$$\vec{H} = (H_0 + H_1^*)\vec{x}_1 + H_2^*\vec{x}_2 + H_3^*\vec{x}_3 \qquad (16)$$

in the magnetic set where the ambient field lies along $\vec{x}_1$. The mixing of modulation is illustrated most simply if we assume that $\theta = \varphi = 0$. Then the signal amplitude is given by

$$\left|\epsilon(t)\right|^2 = (\dot{H}_1^*)^2 + (\dot{H}_2^*)^2 + \omega^2[H_2 + (H_2^*)^2] - 2\omega H_1 \dot{H}_2^* + 2\omega \dot{H}_1^* H_2^* \qquad (17)$$

and the phase by

$$\psi = \tan^{-1} \frac{\dot{H}_2^* - \omega H_1}{\dot{H}_1^* + \omega H_2^*} \qquad (18)$$

It is to be noted that mixed modulation appears in these formulas. For example, amplitude modulation is present when

*It is assumed in the discussion of this section that the turn-area product of the coil is unity.

$\dot{H}_1^* = 0$ and phase modulation when $\dot{H}_2^* = 0$, the former corresponding to the case where amplitude variations in the field are absent and the latter where phase variations associated with Alfvén waves are absent.

The phase modulation of a pure compressional wave is given, from eq. (18), by

$$\psi = \tan^{-1}[\dot{H}_1^*/\omega(H_0 + H_1^*)] \qquad (19)$$

A specific example of probable phase modulation due to an amplitude field taken from an early space probe flight [8] is shown in fig. 10. It is possible to assign the originating signal to a scalar time dependent field in this case since eq. (19) shows a dependence in the denominator upon the ambient field; thus, for fields where the ambient value, $\bar{H}_0$, is sufficiently large, as in the case of the data of fig. 10, it becomes possible to assert that the inverse (i.e., an initial phase modulation) could not have been responsible for the joint modulation of the signal.

For search coils it is possible to remove the ambiguities associated with differentiation by driving two coils in quadrature. This is shown as follows. From eq. (15) the two quadrature signals are given by

$$\epsilon_\alpha = \dot{H}_1^* + \omega H_2^* \qquad (20a)$$

and

$$\epsilon_\rho = \dot{H}_2^* - \omega H_1 \qquad (20b)$$

fig. 10

These expressions being linear differentials can be solved simultaneously, yielding

$$H_1 = (\epsilon_\alpha - \omega\epsilon_\rho)/(s^2 + \omega^2) \tag{21a}$$

and

$$H_2 = (\epsilon_\rho + \omega\epsilon_\alpha)/(s^2 + \omega^2) \tag{21b}$$

where

$$s^2 = d^2/dt^2$$

5.0 Multirate Switching and the Generalized Problem of Alias

From the cases of modulation discussed earlier, especially vector modulation, it is clear that for accurate and undistorted reproduction of large amplitude Alfvén waves the bandwidth extension becomes far greater than for simple scalar modulation of the magnetic field. Truncation of the side band structure in order to satisfy the requirements of the sampling theorem can lead to distortion from the elimination of significant side band energy.

Under the simple conditions imposed by periodic sampling the application of the sampling theorem to band limited data is straightforward. When multirate switching is employed, the sampling problem is greatly increased in complexity. Such sampling is commonly found where data channels are time shared between experiments. That is, the signal channel is alternated between several data sources, with the result that each may be sampled at a high rate for a short time followed by a period of

quiet while the channel is turned to another source. The
fundamental result of multirate sampling is to complicate the
foldover problem greatly as will be brought out later.

5.1 Single Rate Sampling

As a prelude to the multirate case, we now review the
simple periodic switch. The switch function is represented
by the sequence of deltas

$$g(t) = \sum_{n=-\infty}^{\infty} \delta(t - nT_1) \tag{22}$$

repeated at the basic time, T_1. The Fourier transform is the
analog of the time function in the spectral domain

$$G(\omega) = \frac{1}{T_1} \sum_{n=-\infty}^{\infty} \delta(\omega - n\omega_s); \qquad \omega_s = \frac{2\pi}{T_1} \tag{23}$$

Given a sampled time series of data represented by $f(t)$, the
spectrum of the sampled data is then represented by

$$F(\omega) = \frac{1}{T_1} \sum_{n=-\infty}^{\infty} F(\omega - n\omega_s); \qquad \omega_s = \frac{2\pi}{T_1} \tag{24}$$

which means that the original spectrum is duplicated at inter-
vals of $2\pi/T_1$ and bears little resemblance to the original,
except for the form of the replicated spectra. The function
$F(\omega)$ is shown diagrammatically in fig. 11. Aliasing arises when
the data spectrum is extended so that overlap takes place. In
particular for real systems, low pass filtering is employed so
that the overlap between the lowest two spectra is not significant,

fig. 11

although in principle bandpass filtering about higher frequency replicas of the original spectrum would yield the same limitations upon folding. It is clear that the faithful reproduction of hydromagnetic waves must take into account the folding process, and that simple band limiting to guard against overlap may result in side band truncation, especially when a complex PM spectrum is present. If the system is designed for scalar modulation cutoff at some frequency, ν, aliasing will be eliminated at the potential risk of vector modulation side band elimination and distortion of the final signal for Alfvén waves of frequency $\sim\nu$, unless allowed for in the design. For the more complex case, for example, where spin modulation is superimposed upon a complex PM spectrum, spectral folding can cause distortion as spectral components from $n > 0$ may fold into $n = 0$ even though band limiting is carefully considered.

Since the sequence, $g(t)$, represents an idealized case where all the Fourier coefficients are of equal amplitude, the spectrum extends to infinity. In the real instance, finite width pulses are employed (fig. 12). Then the coefficients are altered according to

fig. 12

$$C_n = \frac{\tau}{T_1} \frac{\sin \pi k\tau/T_1}{\pi k\tau/T_1} \qquad (25)$$

where τ is the pulse width and T_1 the repetition time, and the spectrum of the sampler $g(t)$ becomes

$$G*(\omega) = \sum_{k=-\infty}^{\infty} \frac{\tau}{T_1} \frac{\sin \pi k\tau/T_1}{\pi k\tau/T_1} \delta(\omega - k\omega_S) \qquad (26)$$

where $\omega_s = 2\pi/T_1$, and we call the finite width sampler, $g*(t)$.
There is no special significance to this result since interest
centers on the lowest frequencies and generally the formula
with constant coefficient suffices.

5.2 Multirate Switching

This problem is dealt with by one of two methods. Either
the second switching spectrum,* which is now introduced, is
taken as a modulation of the original singly periodic function,
$g(t)$, and the spectral forms are combined, or the function
$g(t)$ is decomposed into separate parts whose phase relation
is considered. In either case the essential question to which
the discussion is addressed becomes the foldover modification
to the low frequency domain of the spectrum.

It is desired to find the Fourier transform of the doubly
sampled function represented by

$$[f(t) \cdot g(t)]g*(t) = \overline{f(t)} \cdot g*(t) \qquad (27)$$

where $g(t)$ and $g*(t)$ are defined in the previous section.
(The switch with finite pulse width, the burst function, is
taken for the function which interrupts the sampling given by
$g(t)$.) The functions $f(t)$, $g(t)$, and $g*(t)$ are delineated

---

*In the following discussion, $g(t)$ will occasionally be
referred to as the sampling function, and $g*(t)$ as the burst
function.

for the time domain in fig. 13. According to the convolution theorem the transform of two functions equals the convolution of the transforms. Applying the theorem to the present case where the periodically sampled function, $f(t) \cdot g(t)$, is modulated by the burst function, $g*(t)$, one has

$$\overline{[f(t) \cdot g*(t)]} = F[f(t)]*G[g*(t)] = F(\omega)*G*(\omega)$$

$$= \int_{-\infty}^{\infty} F(\omega - \Lambda)G*(\Lambda)d\Lambda \qquad (28)$$

Substituting from eqs. (24) and (26) we have*

$$F(\omega)*G*(\omega) = \int_{-\infty}^{\infty} \left[\frac{1}{T_1} \sum_{n=-\infty}^{\infty} F(\omega - n\omega_S - \Lambda) \right]$$

$$\times \left[\sum_{k=-\infty}^{\infty} \left(\frac{\tau}{T_2} \right) \frac{\sin \pi k\tau/T_2}{\pi k\tau/T_2} \delta\left(\Lambda - \frac{2\pi k}{T_2} \right) \right] d\Lambda \qquad (29)$$

With the assumption that proper convergence is observed for the sequences, the summation may be removed from the integral and the integral reduces to

$$\int_{-\infty}^{\infty} F(\omega - n\omega_S - \Lambda)\delta\left(\Lambda - \frac{2\pi k}{T_2} \right)d\Lambda = F(\omega - n\omega_S - k\omega_T) \qquad (30)$$

where $\omega_S = 2\pi/T_1$, $\omega_T = 2\pi/T_2$, and T_1, T_2, τ refer, respectively, to the sample period for $f(t)$, $g*(t)$, and the pulse width for the switch, $g*(t)$. Then

---

*In the multirate notation two periods, T_1 and T_2, appear for $g(t)$ and $g*(t)$, respectively; therefore, in writing eq. (27) using eq. (26), we must consider the time interval T_1 given in that equation as our new T_2.

$$F(\omega)*G*(\omega) = \sum_{n=-\infty}^{\infty} \sum_{k=-\infty}^{\infty} \frac{1}{T_1} \left(\frac{\tau}{T_2}\right) \frac{\sin \pi k \tau / T_2}{\pi k \tau / T_2} \times F(\omega - n\omega_s - k\omega_\tau)$$

$$(31)$$

The terms ahead of F represent a modulation of the familiar form given by the tabulated function $\sin x/x$. This is now a doubly modulated function for which each value of the variable n summation takes place over all values of k. Conversely, one can take the opposite point of view and sum over n for each k. Which choice is made is a matter of convenience arising from the relative periods, T_1 and T_2. For the case at hand, $T_2 \gg T_1$ and one finds that the original replication of $f(t)$ at intervals of T_1 now occurs for all values of k.

It is clear that what has taken place is to replace the replicated spectrum shown in fig. 11b by a new infinity of replications. For each n, k ranges from $-\infty \leq k \leq \infty$. However, the modulation from $\sin x/x$ becomes important and suppresses the lines corresponding to the higher values of k. For simplicity fig. 14 shows only the spectral lines corresponding to the multirate switch $g(t) \cdot g*(t)$. This displays the multiplicity of lines which are generated. The case taken is for $\tau/T_2 = 0.25$, which is for a burst function, $g*$ having a duty cycle of $1/4$.

Next we turn to the application of the above switching spectrum to a data function, $f(t)$, which is arbitrarily band limited according to the singly periodic Nyquist limit given by the heavy line in fig. 15. Here a simple monotonic function

fig. 14

fig. 15

was assumed for the original data spectrum. The duty cycle

for $g*(t)$ is 0.25 as before so that every fourth line is

suppressed. Further, the ratio of repetition frequencies

$T_1/T_2 = 8$ so that the second order $(k = 5,6,7)$ for $n = 0$

lies in the domain covered in the lower figure. These spec-

tral components are not shown because they would further

complicate the diagram. We have also not shown the inversion

where negative frequencies are folded over the positive domain.

Clearly, for the spectra not centered on zero, further compli-

cation would ensue. Therefore, the figure is to be taken as

a lower bound on the folding problem. The region of interest

is picked by the original constraint that the original periodic

(T_1) folding limit be observed. Attention is directed to the

two basic types of alias which take place. The zeroth order

folding about $n = 0$ is shown in the upper figure and results

from the shifting of secondary spectra generated by $k = 1,2,3$.

Since all the energy comes from multiplets of $n = 0$, it is

apparent that this becomes a basic property of multirate

switching. Actually the same argument applies to the first

order shifting for the multiplets of $n = 1$. In this case

much of the energy resides above the intrinsic singly periodic

Nyquist limit and does not enter into the pass band. However,

some energy is folded down and must appear in the data band.

Little can be done to eliminate folding from the multirate

case unless the multiplet structure is collapsed. This can

only take place when the repetition frequency is decreased;

in the limit this frequency approaches the original singly
periodic rate. The actual error introduced into the shape of
the spectrum depends in an important manner upon the true
spectral function of the data. Thus it becomes impossible
in a self-consistent way to determine the spectrum from the
aliased case.

Some general rules can be found from the above discussion.
Decreasing the duty cycle may be helpful since this factor
enters in the amplitude of the multiplet structure. However,
higher order multiplets appear within the domain of n = 0
and the first zero of the subsidiary structure is not attained
quickly. Thus, although the amplitudes of the multiplet
spectra are reduced, the terms damp more slowly. The other
variable at the disposal of the designer is the sampling ratio
for the functions g(t) and g*(t). As indicated above, this
implies turning on the basic periodic switch, g(t), less often;
this is at the expense of information rate. In this instance
the multiplet structure shrinks in the frequency domain and
higher order terms of both positive and negative sign, accord-
ing to the value of sin x/x, appear within the data band.
Some cancellation of terms will take place, and since the
higher order spectra are down in amplitude, they will not
make important contributions to the final spectrum.

The situation found for the double rate switch is mathe-
matically similar to Fraunhofer diffraction and appeal may
be made to physical optics for an analogy. In the earlier

discussion of spectral folding, the higher order contributions to $\sin x/x$ were ignored so that the pictorial representation would not become forbiddingly confusing. Actually, the intensities of these maxima are not especially important to the folding problem as they are distributed in the following way:

$\dfrac{k}{T_2}$	Maximum
0	1
$\dfrac{3\pi}{2}$	$(2/3\pi)^2$
$\dfrac{5\pi}{2}$	$(2/5\pi)^2$
$\dfrac{7\pi}{2}$	$(2/7\pi)^2$

5.3 The Switching Function in Vector Space

Before turning to the simulation of the concepts discussed earlier, an alternative representation of the switching function is given here. This will provide a direct means of measuring the amplitude of the various terms in the switch spectrum. It also facilitates the view of the relative importance of the different contributions toward a particular spectral component.

In the framework to be discussed in this section, the basic argument employed is the shifting property of the Fourier transform. In the language of communication practice we consider an interrupted set of sampling pulses as given in fig. 16 which shows j equi-interval pulses followed by a blank period, corresponding to the earlier case of double sampling where the

fig. 16

periodic switch $g(t)$ was modulated by the burst switch, $g*(t)$. The j samples are contained in the time jT_1 and the basic repetition rate is given by the period, T_2. The sampling pulses are taken in the narrow limit so that the sequence is represented by eq. (22).

Now consider the case where $g(t)$ is replaced by a sequence of functions each of the form $g(t)$ but time shifted. Thus $j = 1$ represents the first term of a sequence of deltas repeated at intervals of T_2. Each of the remaining pulses in the series j is also the first member of a new sequence. What we have done is merely to sum the sequence, $g(t)$, differently as follows:

$$\overline{g(t)} = \sum_{m=1}^{\infty} \delta(t - \Delta - nT_2) + \ldots + \sum_{n=1}^{\infty} \delta(t - j\Delta - nT_2)$$

where the repetition interval T_1 is replaced by T_2, $q\Delta$ is the time lag for the qth subsequence where $1 \leq q \leq j$ and $\Delta < T_2$; therefore

$$\overline{g(t)} = \sum_{q=1}^{j} \sum_{n=1}^{\infty} \delta(t - q\Delta - nT_2) \tag{32}$$

From the shifting theorem the companion transforms are given by

$$\overline{G(\omega)} = \frac{1}{T_2}\left\{ \sum_{n=-\infty}^{\infty} \delta(\omega - n\omega_s)e^{2\pi i\Delta\omega} + \ldots + \sum_{n=-\infty}^{\infty} \delta(\omega - n\omega_s)e^{2\pi ij\Delta\omega} \right\}$$

$$= \frac{1}{T_2} \sum_{q=1}^{j} \sum_{n=-\infty}^{\infty} \delta(\omega - n\omega_s)e^{2\pi iq\Delta\omega} \tag{33}$$

where q and Δ are as defined in the case of $\overline{g(t)}$.
Therefore each spectral line from each of the sub-sequences
has a characteristic phase. It is the vector addition of
the contributions from the different sub-sequences to each
of the spectral components which determines the relative
strength of that line. Thus for the cancellation of certain
spectral components from the switching spectrum it becomes
clear that the procedure to follow is to make all the contri-
butions from the different sub-sequences cancel.

It is possible to represent these contributions by a
vector plot which will be unique for each of the spectral
components. An example is given in fig. 17 which shows the
distribution of components from the different sub-sequences.
The problem is similar in certain respects to that encountered
in the simple theory of diffraction. It is seen immediately
that for cancellation of a certain spectral line, the vector
distribution over the circle of radius $1/T_1$ must be uni-
formly dense. Further, the largest contribution to a spectral
line takes place when the vectors are distributed over one
quadrant or less. Distribution over more than one quadrant
tends to damp the net strength of the line. Each of the har-
monic components in the total spectrum is determined by its
vector diagram in like fashion. Since the contributions
become periodic in times greater than T_2, it is necessary
only to consider the contributions generated from the first
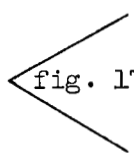
fig. 17

members of the train of sub-sequences. In the synthesis the reordering of $g(t)$ into sub-sequences means that for each sub-sequence the characteristic time becomes T_2 rather than T_1.

In the representation given in this section, the fundamental view is that one begins with a sequence having a characteristic time, T_1 and removes first one pulse at a repetition period of T_2. This immediately introduces spectral components at the frequency characteristic of T_2, namely $2\pi/T_2$. These components shrink or grow according to the arguments given here. The relative magnitude of the various contributions to the total spectrum can be obtained by a simulation as is shown in fig. 18 which gives the events when a periodic sequence is interrupted by removal of members of the set whose basic frequency is 5 in arbitrary units. A new periodicity equal to 1/5 is introduced.

fig. 18

6.0 Sequential Vector Sampling

So far all the arguments developed have tacitly bypassed the fact that measurement of magnetic fields is customarily carried out by sampling the three components separately. Any proper measurement will, of course, require that both the field magnitude and direction be known so that three quantities are required in the general case, whereas the earlier discussion assumed that a scalar time series was involved in the data transformation process.

It is assumed first that we are dealing with a time
stationary spectrum and that aperiodic phenomena such as
sudden changes in the field are absent. Later the transient
case will be considered. For the purpose of this discussion
the magnetic field is divided into three orthogonal components
whose values individually are given as three time series linked
by the field equations. Sampling of each of the component time
series is taken to occur as before, using $g_i(t)$ where
$i = 1, 2, 3$. The switching functions g_2 and g_3 are shifted
in time, respectively, from g_1 by T_1 and $2T_1$.

In the limit of periodic sampling, measures are taken at
the rate $2\pi/T_1$; however, for any one component, the frequency
interval is $2\pi/3T_1$. In the other extreme, an additional
modulation or blanking function $g*(t)$ is added to the ensemble
where the on-time for $g*$ is arbitrarily taken to be $3T_1$.
This corresponds to sampling the total field at intervals T_2,
each sample comprising the three components separated by inter-
vals of T_1. (The addition of more samples during the on-time
of $g*$ would lend little to the discussion and is therefore
not considered.)

For either of the two limit cases proposed, the sampling
is divided as in the last section into sub-sequences, each
sub-sequence representing measurements from only one sensor.
It is clear then that the basic sampling rate for each sub-
sequence is given by $2\pi/T_2$ independently of T_1 and that

the latter quantity has no bearing on the proper value for Nyquist band limiting. Further, if this alias-free limit is to be observed, then, for either extreme given above, the Nyquist limit categorically removes the possibility of sample error due to nonsimultaneity of sampling. This would clearly not be the case if the constraints stated before were violated.

The correlation functions or convolution integrals are related to the transforms in the following manner

$$\int_{-\infty}^{\infty} H_i(t) H_j(\tau - t) dt = F[H_i(t)] F[H_j(t)] \qquad (34)$$

where H_i, H_j, and H_k are the field components and F represents the Fourier transform. It is not possible for the band-limited correlations to be affected by the switching sequence for their associated Fourier transforms are band limited by the alias-free requirement. Thus sequential sampling is allowed without data distortion under the guidelines laid down above. This in no way absolves the earlier limitations regarding multirate aliasing. The allowance of sequential sampling in the presence of multirate alias and band shifting requires examination but is outside the scope of this paper.

We now turn to the case of transients in the field. It is simplest to take the case of the step function. We must define the step according to whether it is a change in the magnitude or direction. The step will be taken to be a contact surface such that the magnetic field can excite a jump in magnitude for the simple case where no change in direction

(skewing) takes place. The component measures of the field all vary together and are linked simply by the resolution of the field. Thus the response of the three detectors will lag in time according to eq.(32) and their transforms by the phase as expressed in eq. (33). The important thing to observe is that the time domain is apparently reversed because the last detector to see the discontinuity becomes that reading the signal nearest the origin. Because of the phase shifts in the spectra, the contributions from the three sensors must be combined by observing the complex coefficients of the Fourier integral of the discontinuity. Thus, for example, the net amplitude spectrum is computed using the complex arguments. However, again as before, if the Nyquist criterion is observed, important contributions to the spectrum cannot be generated in the domain where phase shifting is important. For the low frequencies below the Nyquist cutoff, the phase shifts become small and the contributions from the three components of the field tend toward zero phase difference. The error will diminish as the frequency cutoff is lowered according to eq. (33). The allowable error in the spectra is then the determining factor whether sequential sampling is permissible.

7.0 Synchronous Demodulation From Spinning Spacecraft

In order to remove one source of modulation from data obtained from spinning spacecraft, it is possible to demodulate using an inertial or nearly inertial reference such as the sun.

Such a procedure requires that the generation process contain
information which is in time quadrature. A particular example
applies to magnetometers wherein the sensors are so arranged
that they generate signals which are phased by $90°$, as when
orthogonally positioned on the spacecraft. When the two sig-
nals are each multiplied by sine and cosine replicas of the
spin signal, the rotational modulation can be shown to cancel
completely with a reduction of the signal spectrum to that
obtained with inertially stable spacecraft.

It can be shown easily that an arrangement as given in
fig. 19, where both the sine and cosine outputs from magnetom-
eter sensors are each multiplied by sine and cosine terms at
the spin frequency, will suffice to remove the spin modulation
from the signal spectrum [9]. Simulation can be made
using an analog computer where the machine is fed a set of
quadrature signals which functionally represent that obtained
from a set of orthogonal magnetometers rotating in a static
field. To the input are then added either or both amplitude
and phase variations which represent the physical situation
where compressional and/or Alfvén waves are present. Such a
simulation demonstrates that any frequencies associated with
field fluctuations are recovered even though they may extend
through and beyond the spin frequency of the spacecraft. The
primary restriction becomes that of the internal bandwidth of
the demodulation system. This must be able to transfer fre-
quencies well beyond those representing the variations in the
field because of the generation of a rich side band structure.
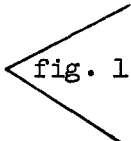
fig. 19

In figs. 20 through 22 are shown the sensor output from one axis, the demodulated sine and cosine outputs, and the associated spectra as determined from a wave analyzer. The case shown is scaled up in frequency for convenience. It represents an Alfvén wave having phase excursions of $\pm\pi/2$ radians at a frequency of 5 cps superimposed upon a spinning system with a rate of 16 cps. The appearance of these spectra is different than those cases hypothesized earlier where the negative frequency domain was employed. Thus in the present case the spectra are found folded according to the way the power is distributed. No loss of generality ensues but the interpretation becomes less straightforward. Figure 23 shows the Lissajou representation of the demodulated wave corresponding to the vector or phase modulation of the original ambient field.

Lastly, to demonstrate the recovery of signals under extreme conditions, an especially pathological time function was introduced into the computer. In this instance the spin frequency was half that of the modulation. Both amplitude and phase modulation were simultaneously superimposed upon the static field. The frequencies were identical for reasons of simplicity of recording. The amplitude variation varied the base field from zero to $2B_o$ causing extreme variations. The phase variations were through $\pm\pi/2$ radians. The impact of such extreme excursions upon the field is shown in fig. 24

which is a Lissajou figure of the signals taken from the output

of the quadrature sensor simulators. The undriven signal would

have been circular, representing the rotating field. Single

axis waveform is shown in fig. 25 and the original input repre-

senting the nonrotating field is shown in fig. 23, which accurately

represents the output of the spin demodulator system. Thus,

complete recovery of this pathological signal at twice the spin

frequency was attained.

fig. 25

Demodulation of the type discussed here need only be carried

out on the spacecraft when the maximum bandwidth is insufficient

to transmit nontruncated signals to earth. From the earlier

discussion, it is clear that spurious signals can, in principle,

always be generated over a restricted range in frequency for

any system. To avoid this it is essential that space demodu-

lation be employed.

8.0 Conclusions

The general problem of the correct reproduction of the time

series created by signals from magnetometers which detect

hydromagnetic radiation together with the correct specification

of the spectra of such fields is found to place two general

constraints upon the design of magnetometer sensor systems.

These have to do first with the generation of modulation from

the beating of the signals with the spin of the spacecraft in

the event the latter is stabilized by rotation, and secondly

by the process commonly employed where the telemetry system

is shared in time multiplex fashion between several experiments.

It is obvious that simple design constraints can eliminate these problems. However, the conceptual simplicity of these constraints is not usually met in practice due to a variety of circumstances mostly having to do with weight and communication limitations. To eliminate the problem of spin modulation of either type discussed in this paper requires merely that time quadrature signals be returned from the spacecraft and demodulated synchronously at the receiving station. The scheme shown for use in spacecraft is equally applicable on the ground. Generally such a practice cannot be carried out because of communication limitations; that is, the signal bandwidth is insufficient to transmit the side band structure. It is clear that demodulation aboard the spacecraft is more economical of bandwidth in any instance. Further, the general requirement that quadrature signals be available is mandatory for demodulation either on the ground or in space, irrespective of the available bandwidth. (For search coils the requirement of quadrature sensor signals is present for any frequency as a result of the inherent differentiation.) For vector or Alfvén wave modulation, the problem becomes more complex. A practical rule to observe is the employment of synchronous demodulation whenever a hydromagnetic radiation field is expected to be encountered.

In regard to the second basic problem posed, that of multirate sampling, here the general rule to observe is to

periodize the data sampling procedure and employ buffer storage in the event that the telemetry system is time shared. The other recourses are either to adjust the switching functions for minimum tolerable folding, which is expensive of bandwidth, or to use multichannel telemetry such as the classical FM/PM system employed in early spacecraft.

As noted early in this paper, questions generated by the existence of spin modulation apply equally to other forms of data collection where angular scanning is employed and physically real conditions exist for the presence of data frequencies that encompass the spin rate.

In conclusion it should be pointed out that the most general type of radiation field will be composed of a mixture of Alfvén and magnetosonic waves. Under the assumption that the system response is linear, the side band structures from the different types of modulation can be linearly superimposed. Since the amplitude spectrum contains only two components which are phased with the carrier and these are of the same frequency as the first two side bands from the vector modulation, the spectral components merely add algebraically. The final modulation is made asymmetrical but is unfolded in the spin demodulation process. Therefore, so long as linearity is preserved, the mixing introduces only academic considerations.

Lastly, although the problem of the spectral content of hydromagnetic signals can be dealt with in a straightforward manner by calculation in the spectral domain, inversion back to the time domain in which measurements are carried out becomes difficult because of the loss of phase information when transforming. Phase is not recovered by the inverse transformation. Though detailed investigation of short swaths of multisampled data is possible and deductions made regarding wave properties, the problem of spin modulation is still present for spin stable spacecraft and cannot be disregarded even in the time domain.

Acknowledgements

References

1. A. R. Sims, Effect of Free Precession and Varying Magnetic
    Field Upon Magnetometer Signals and Aspect Indicator,
    TM 59-0000-00351 (unpublished), Space Technology Labs,
    Los Angeles (1959)

2. C. P. Sonett, Experimental Physics Using Space Vehicles,
    Chap. 1, Adv. in Space Science, vol. 2, Ed. F. W. Ordway,III;
    Academic Press (1960)

3. H. Goldstein, Classical Mechanics, Addison-Wesley, Cambridge
    (1951)

4. M. Schwartz, Information, Transmission, Modulation, and
    Noise, McGraw-Hill (1959)

5. C. P. Sonett, L. Davis, Jr., and P. J. Coleman, Some Aspects
    of the Internal Structure of a Solar Flare Plasma Cloud,
    J. Phys. Soc. Japan 17, Supp. A-II, (1962) p. 524

6. N. F. Ness, C. S. Scearce, and J. B. Seek, Initial Results
    of the IMP I Magnetic Field Experiment, J. Geophys. Res. 69
    (1964) p. 3531

7. C. P. Sonett, The Distance Geomagnetic Field, 2: Modulation
    of a Spinning Coil EMF by Magnetic Signals, J. Geophys.
    Res. 68 (1963) p. 1299

8. C. P. Sonett, A. R. Sims, and I. J. Abrams, The Distant
    Geomagnetic Field, 1: Infinitesimal Hydromagnetic Waves,
    J. Geophys. Res. 67 (1962) p. 1191

9. W. J. Kerwin and R. Muñoz, A Demodulation System for Vector
    Measurements From a Spinning Satellite, presented at the
    Symposium on Signal Transmission and Processing, May 13-14,
    1965, Columbia Univ., New York.

FAST WAVE: $\sqrt{A^2 + C^2}$

SLOW WAVE

H

Q

A-34441-1
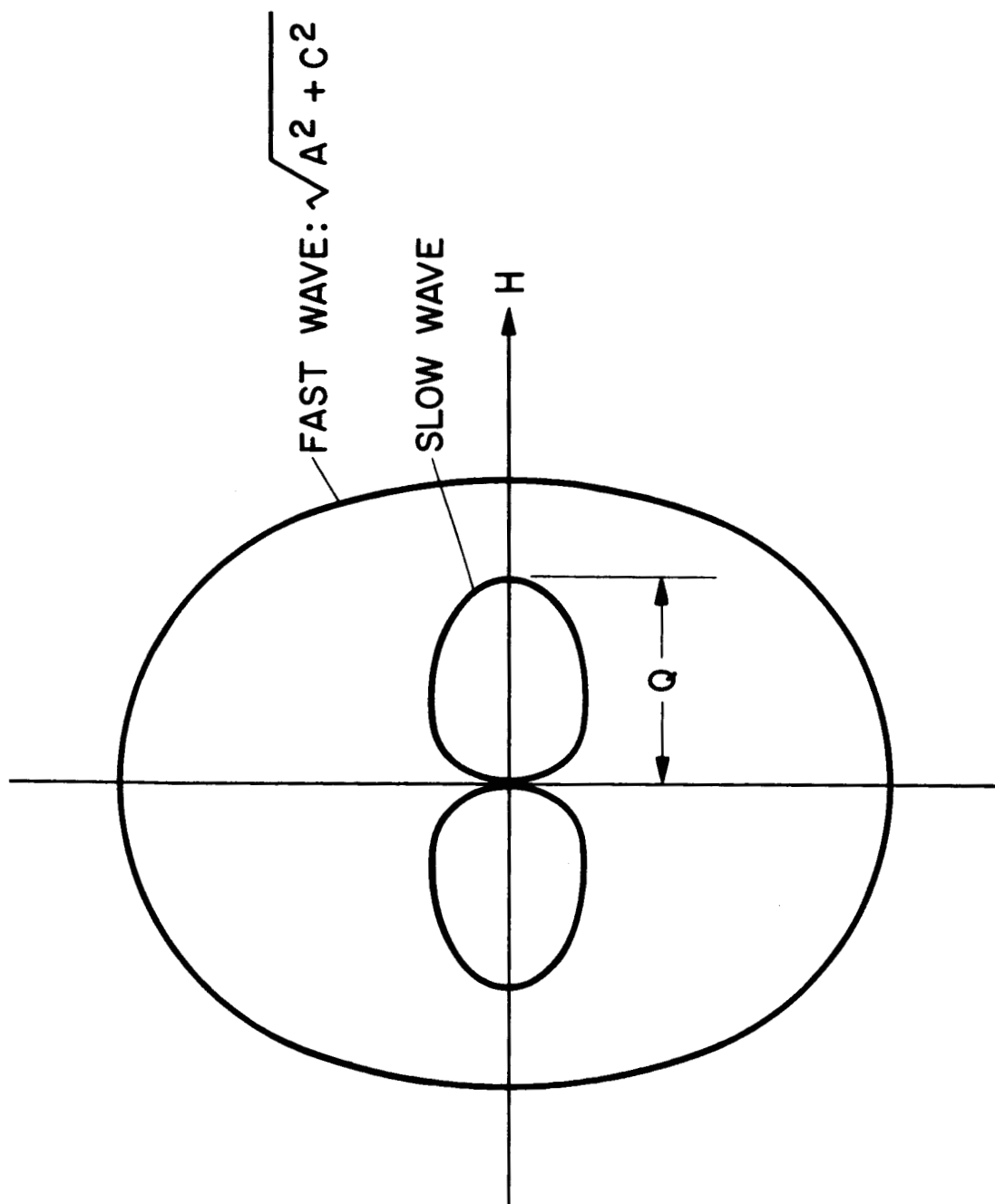
Figure 1.- Surface of constant phase for the fast and slow modes. The quantity A is the Alfvén velocity, C is the sound velocity, and Q is defined as the smaller of the sound and Alfvén velocity. The semiminor axis of the outer ellipse is given by the larger of the two velocities. The Alfvén velocity surface is not shown.
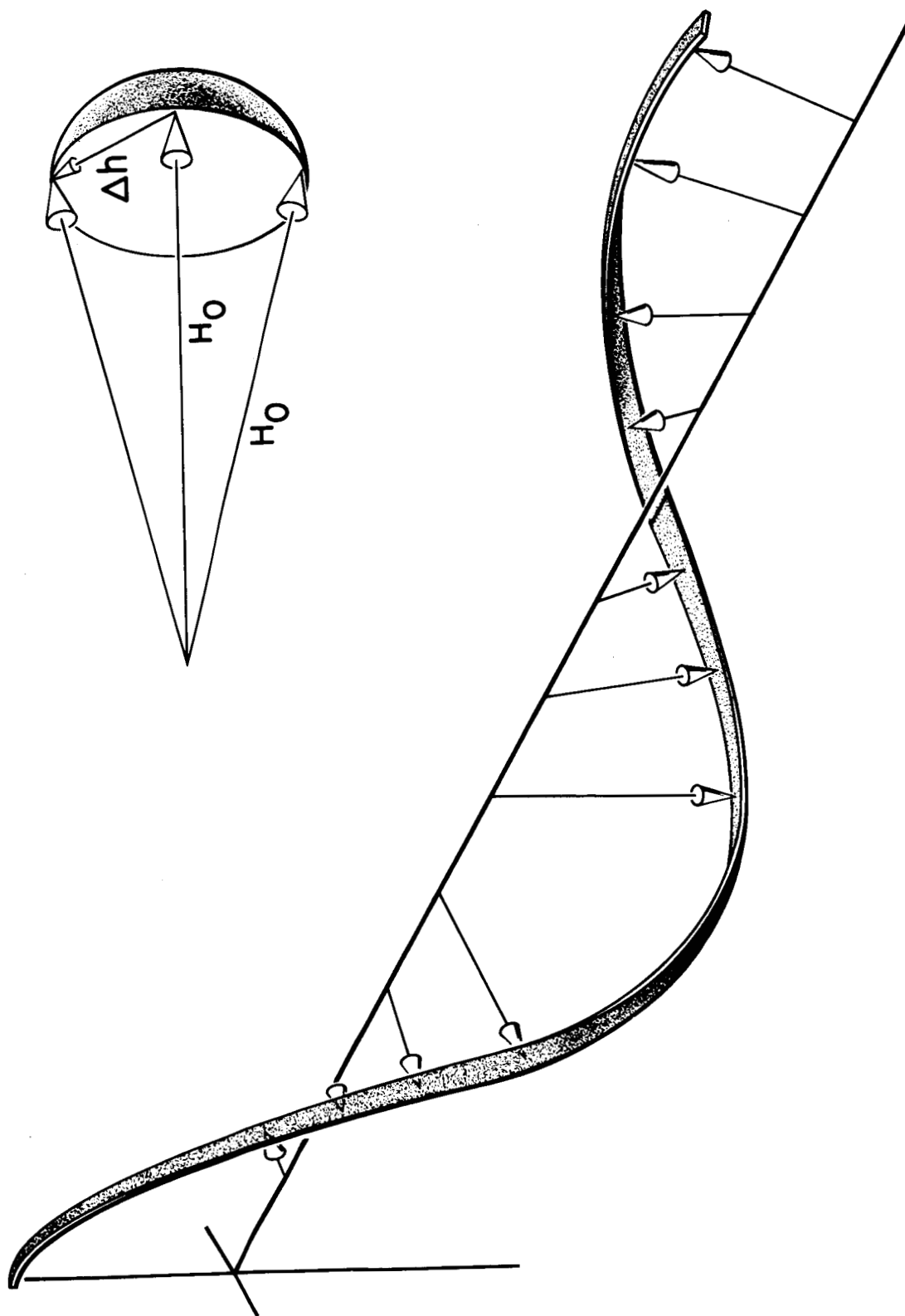
Figure 2.- Rotation of polarization plane for the Alfvén wave. Above gyro cutoff, circular frequency is equal to gyro frequency.
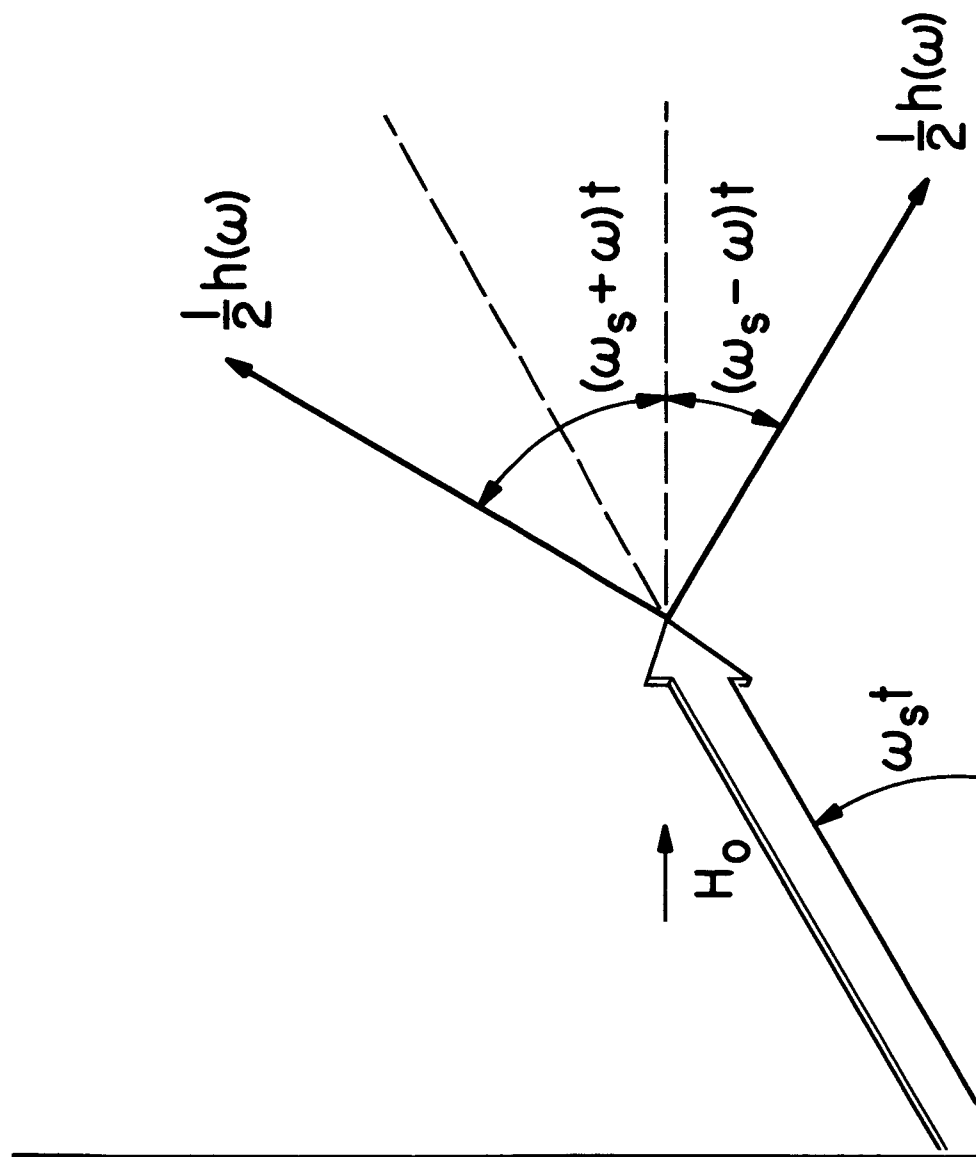
Figure 3.- Vector representation of the terms of eq. (7). The two modulation vectors representing the side bands rotate oppositely and with equal velocities with respect to the frame in which $\bar{H}_o$ is stationary, at the rates $\pm\omega$. Thus the quadrature components cancel always and the modulation is strictly amplitude. If $\omega > \omega_s$ the lower vector rotates in the backward direction with a higher rate than H_o. Nevertheless, the phase coherence between the two side band vectors is preserved.
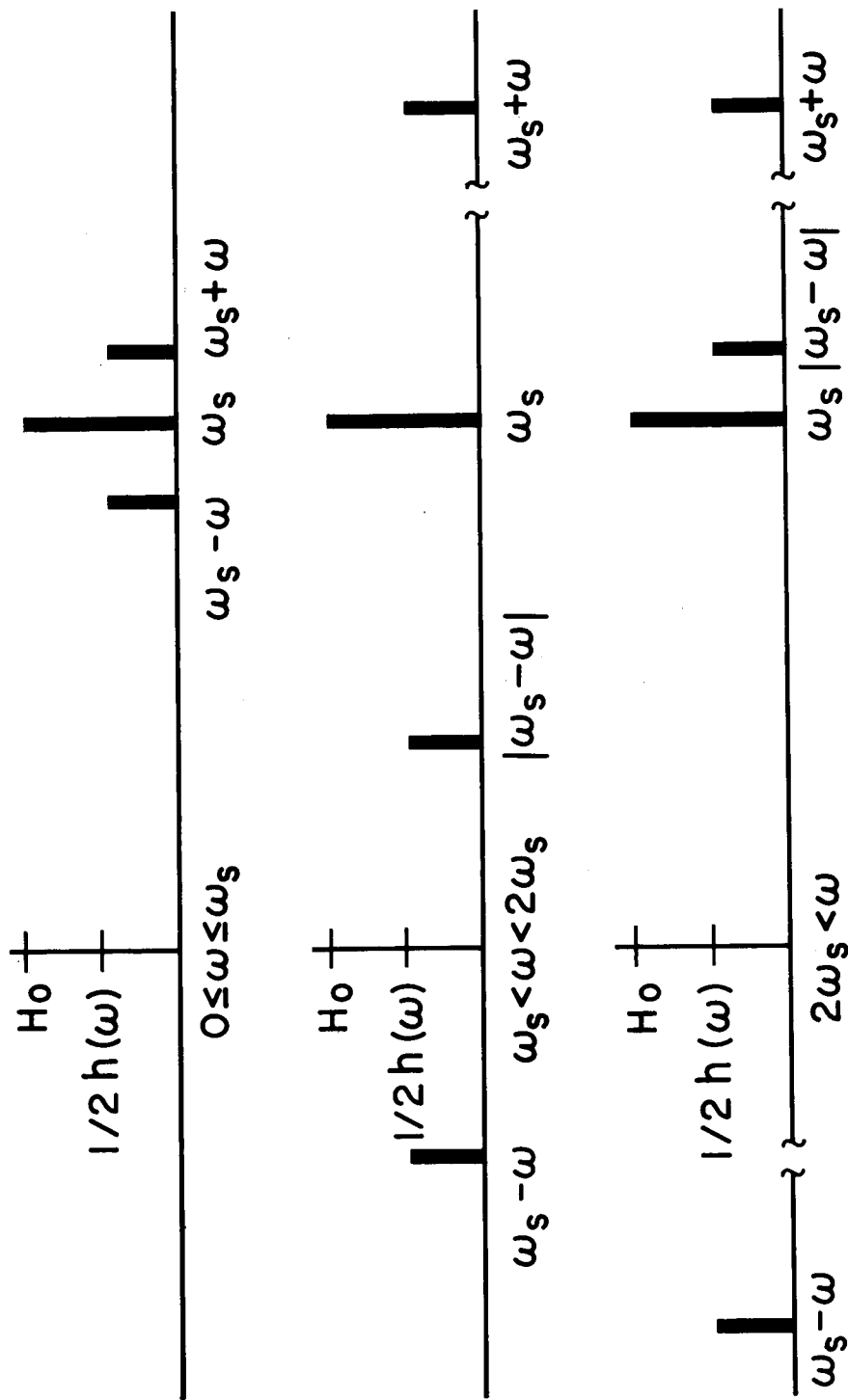
Figure 4.- AM side bands for the three cases discussed in the text, the first being where $\omega \ll \omega_s$, the second where $\omega_s < \omega < 2\omega_s$, and the third case where $\omega > 2\omega_s$. Folding about zero frequency introduces asymmetrization of the side band structure. The lower side band is shown both in the negative frequency domain as well as folded.
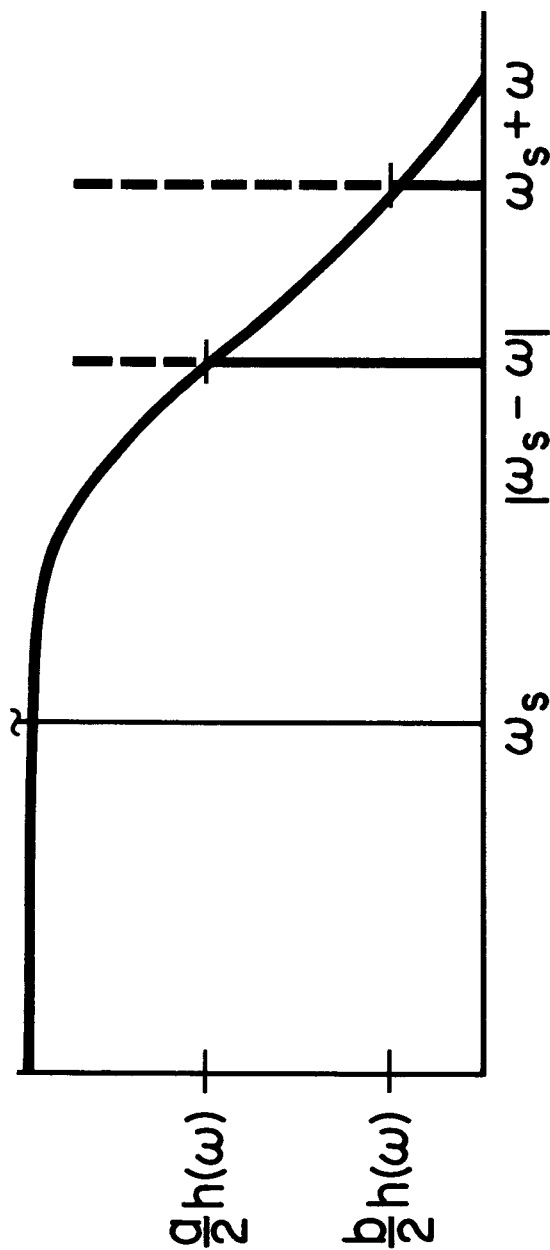
Figure 5a.- View of the asymmetric truncation of the side band structure for amplitude modulation when $\omega \gg \omega_s$. The case shown is for a system filter response with finite slope.
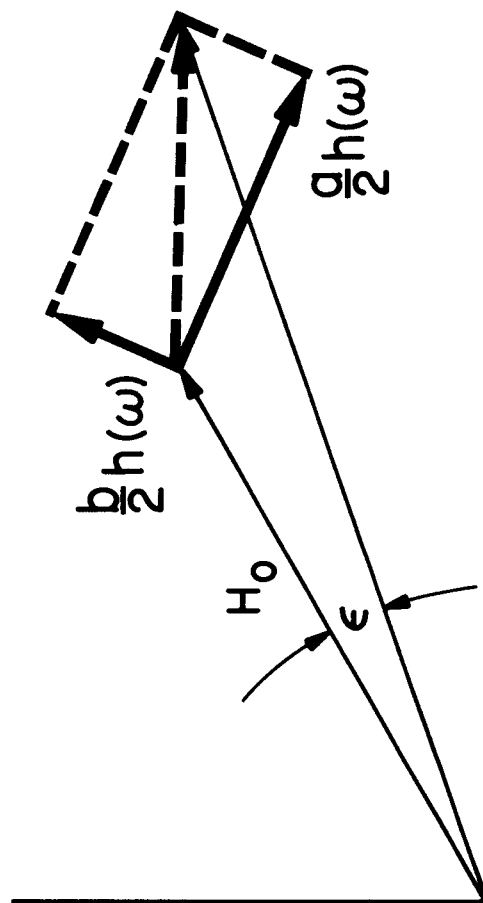
Figure 5b.- Qualitative illustration of how phase modulation is introduced by the truncation process. The side band vectors are no longer of equal amplitude, with the result that H_0 is phase modulated with the instantaneous angle ϵ.
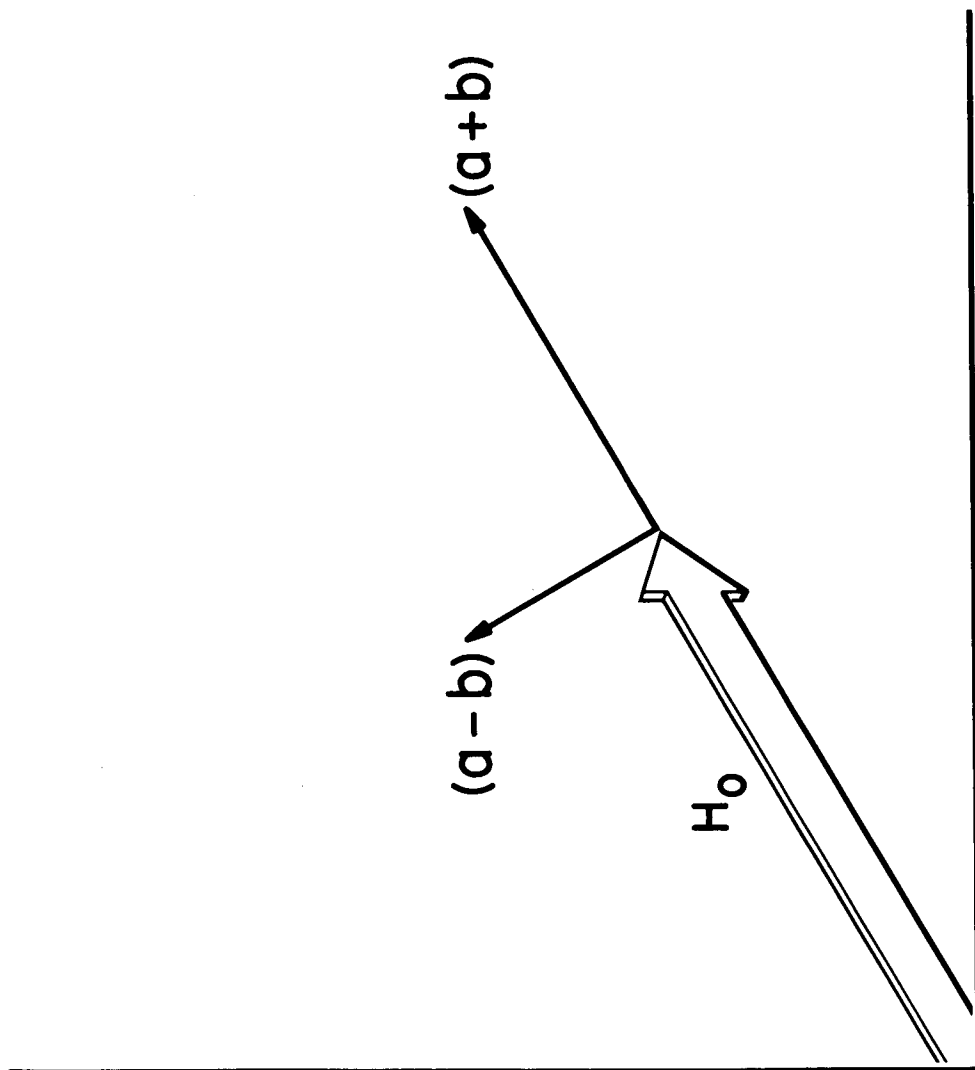
Figure 6.- Results of the assymmetrical side band vectors of fig. 5 into in-phase and quadrature components involved in the frame of reference in which H_0 is constant.
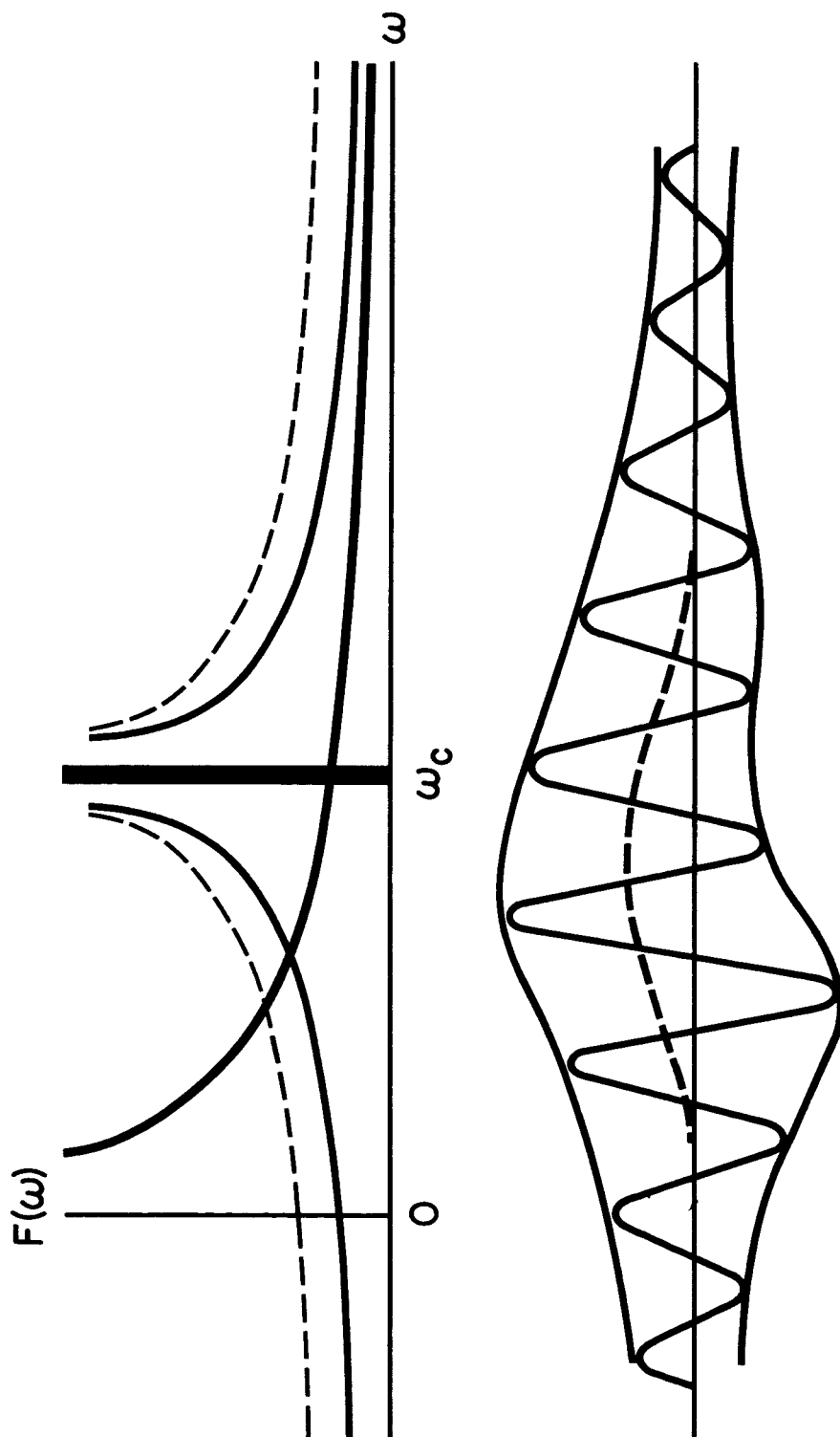
Figure 7.- Idealized spectral domain for a step function associated with a reversal of field. The original step spectrum and the shifted spectra are shown in the upper figure. The lower figure shows a qualitative view of a magnetometer sinusoid modified by passage through a step discontinuity. Both an envelope change and a zero shift take place.
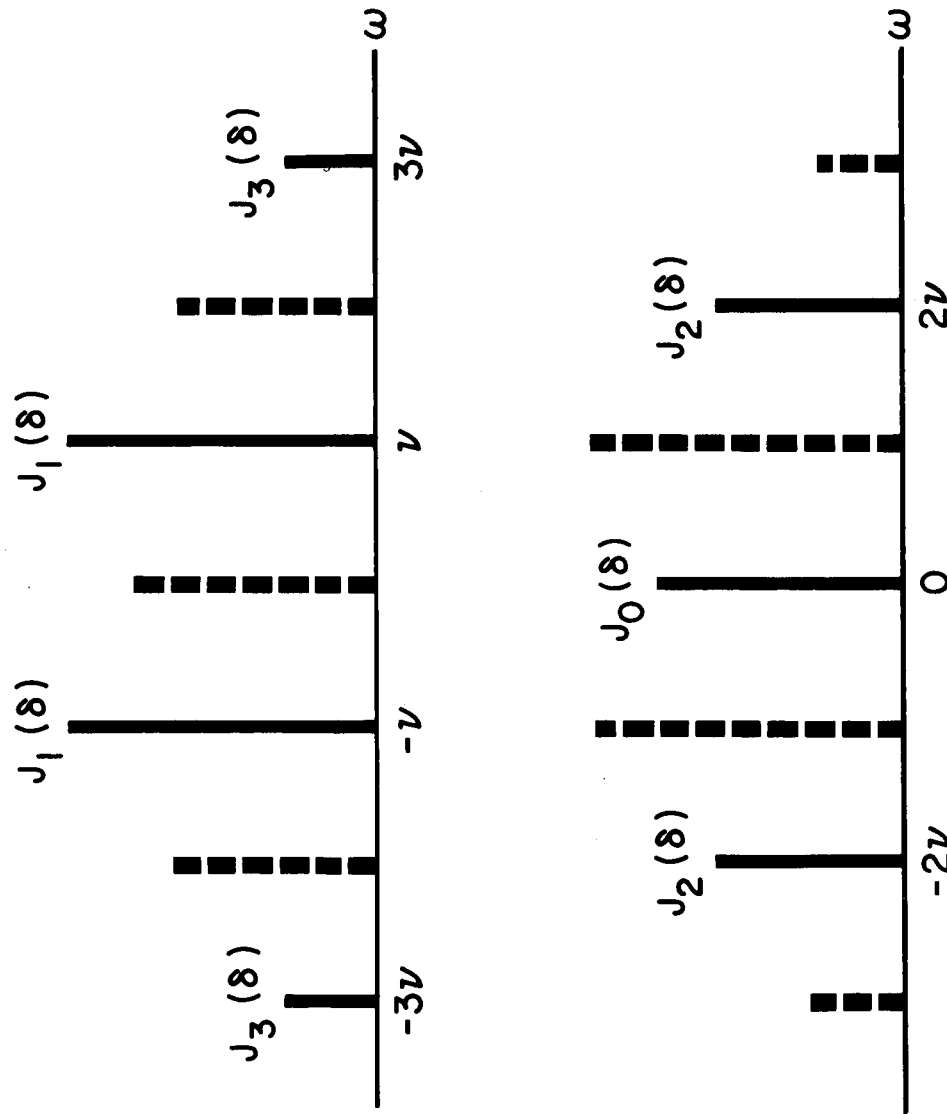
Figure 8.- Side band spectrum for a monochromatic Alfvén wave having the deviation discussed in the text. The upper figure represents the structure for $H_{1,2}$ and the lower for H_3 as given in eqs. (13). Components beyond J_3 are below 1 percent of the carrier in amplitude. Since the modulation is about zero frequency, the spectrum extends into the negative frequency domain, the lines fold over and account for the factor of 2 appearing in eqs. (13). In ordinary phase modulation the spectra are distributed about a nonzero carrier. Thus the fact that the odd side bands are in time opposition about the carrier produces a condition different from the above case where the spectra fold about zero and add in power in spite of the opposed phase.
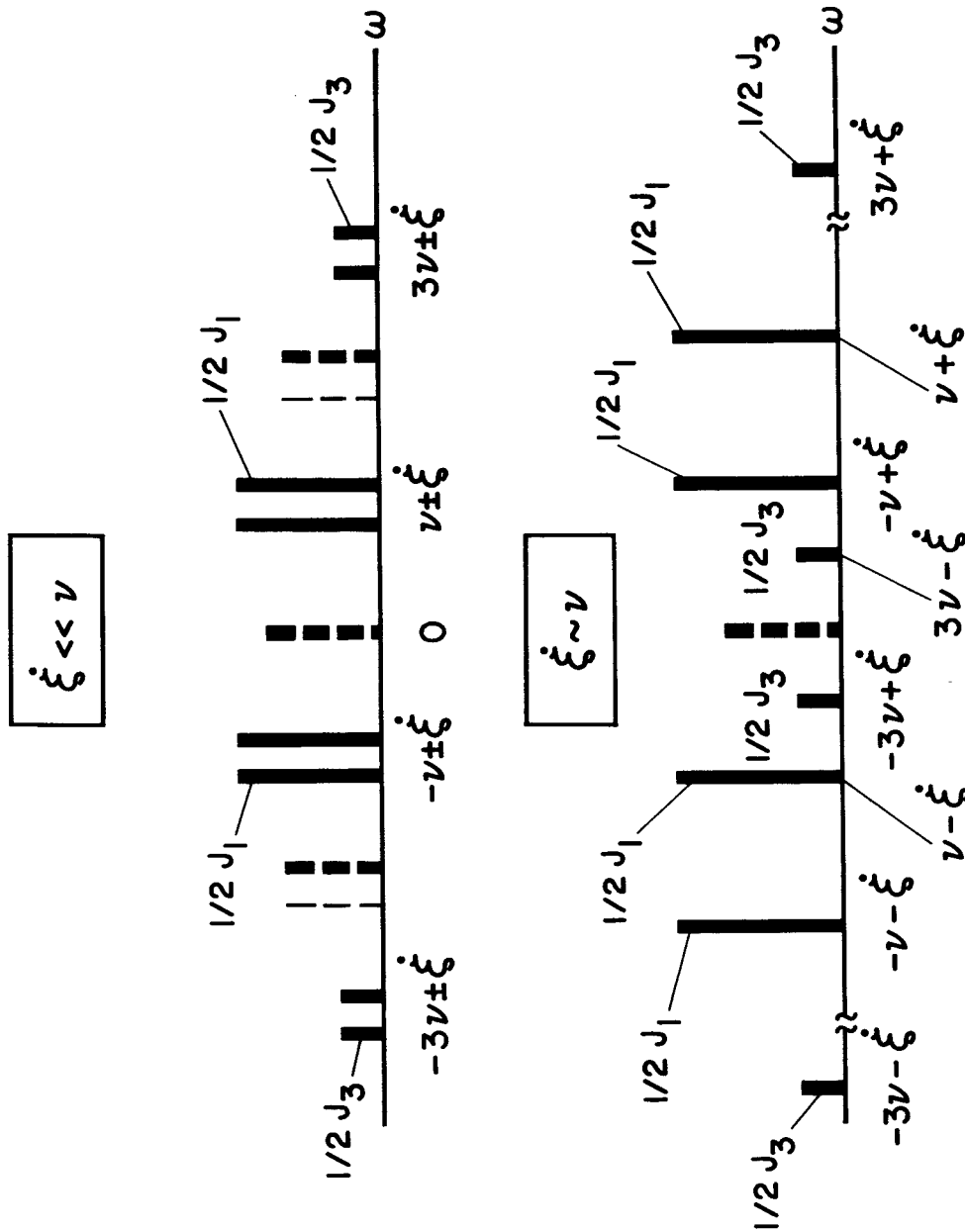
Figure 9.- Upper diagram shows the splitting of the spectral components for $H_{1,2}$ from the beating of the spin frequency with the Alfvén wave spectrum. Each line is half the former amplitude. The lower figure shows the spreading and asymmetrization of the spectrum for the case where the spin frequency is of the order of the modulation frequency. Mapping about zero frequency occurs as the lines shift position. Whereas in the upper spectrum the right- and left-hand sides are in time opposition, in the lower spectrum the phases are scrambled with respect to zero frequency. Thus the ensuing time function is greatly complicated as the power is not simply additive as in the case cited in fig. 8.
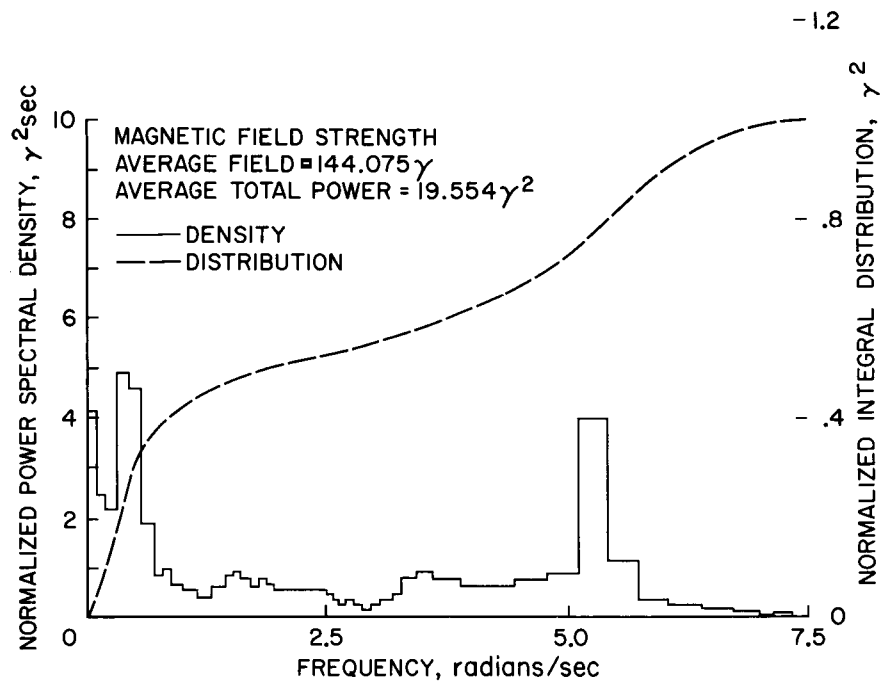
A-34441-10
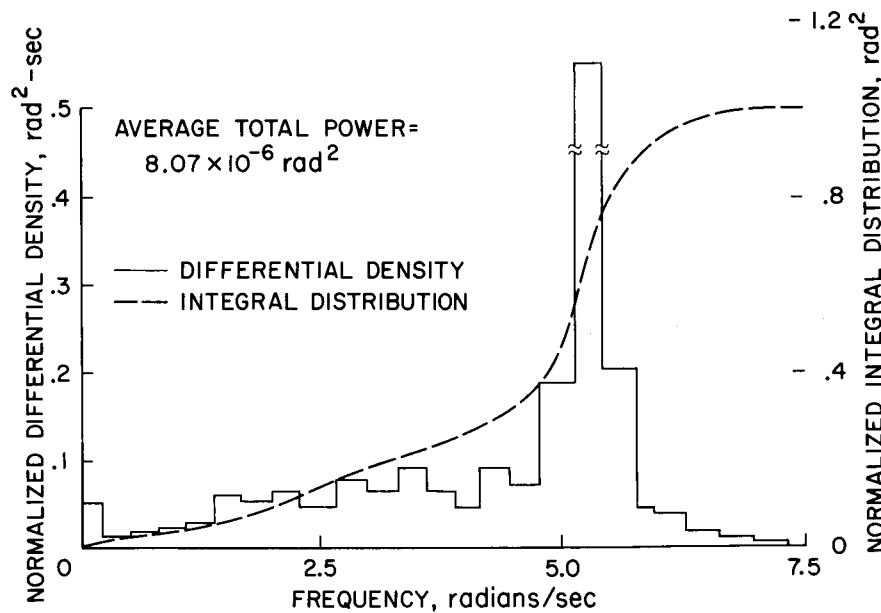
A-34441-11

Figure 10.- Hydromagnetic spectrum of the earth's field at 0 - 7.5 radians per second taken with a single search coil at approximately 7 earth radii on October 11, 1958. Both the integral and differential spectra are shown. It is suspected for the reasons given in the text that the strong line at 5 radians per second in the phase spectrum (fig. 10b) is due to pseudo Alfvén wave generation [8].
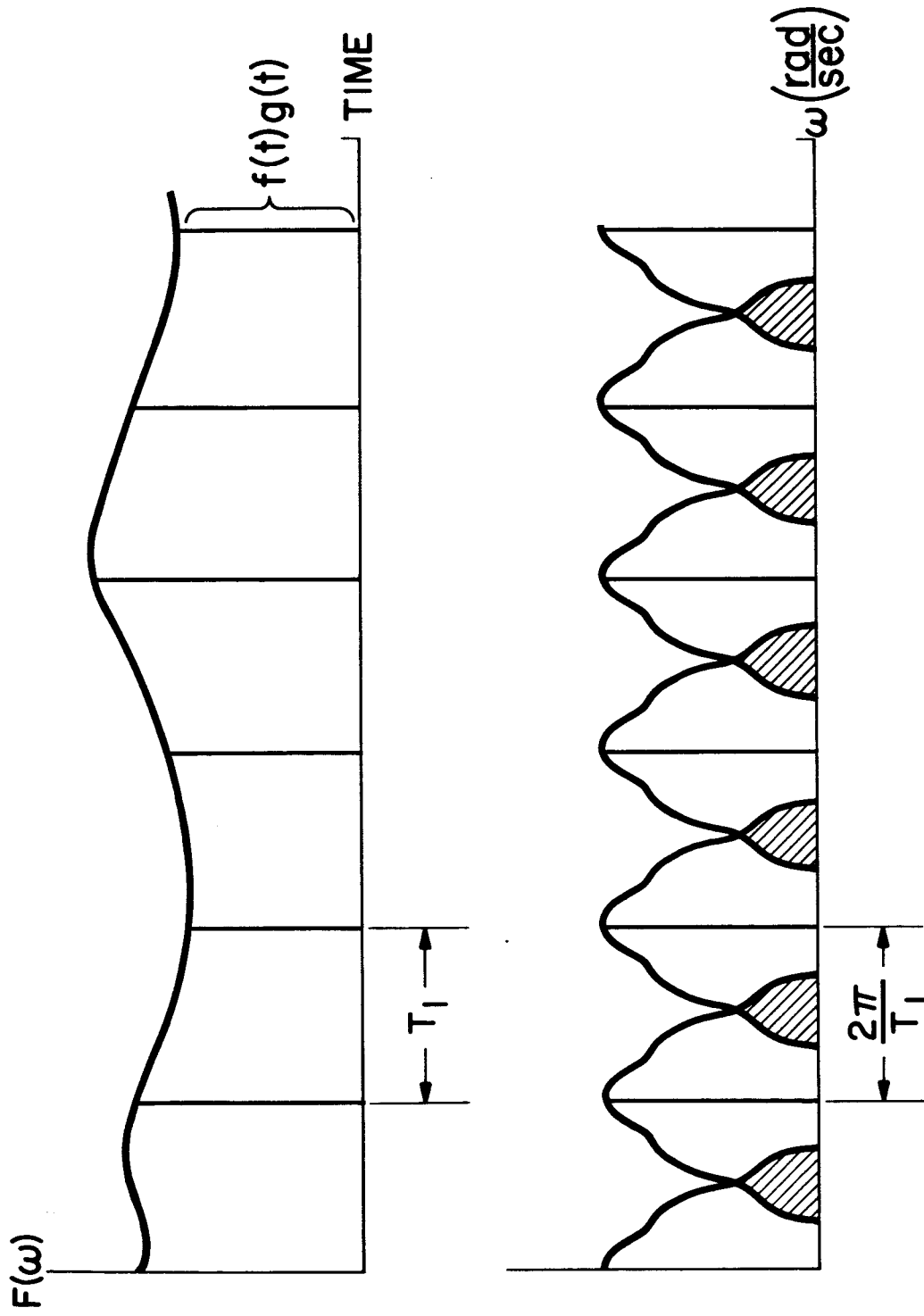
Figure 11.- Upper figure denotes time domain for the function $f(t)$ and the sampling function, $g(t)$. Lower figure shows the replicated spectra for the case of the idealized delta function switching case. The case shown displays some alias.
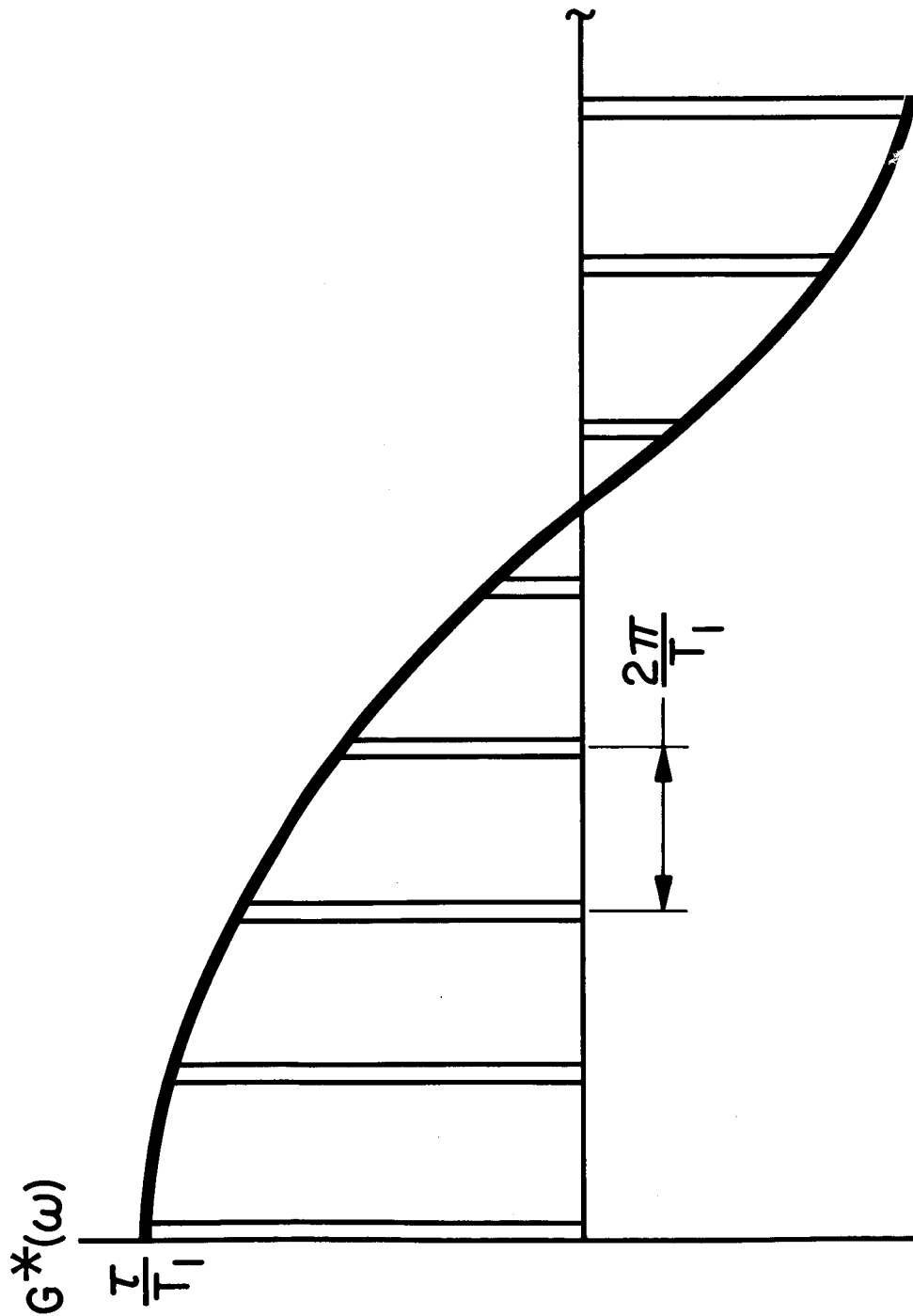
Figure 12.- Spectrum of the sequence consisting of an infinite train of finite width pulses (burst function). The amplitudes and phases are modulated by the term $(\tau/T_1)[(\sin \pi k\tau/T_1)/(\pi k\tau/T_1)]$. Convolving this function with the periodic switch, $G(\omega)$, produces a sequence which gives the multiperiodic spectrum. Note that in this figure the pulse interval is T_1. When developing eqs. (28) through (31) the above function interval is labeled T_2 to distinguish it from the interval of the periodic switch, $G(\omega)$, whose interval is time T_1.
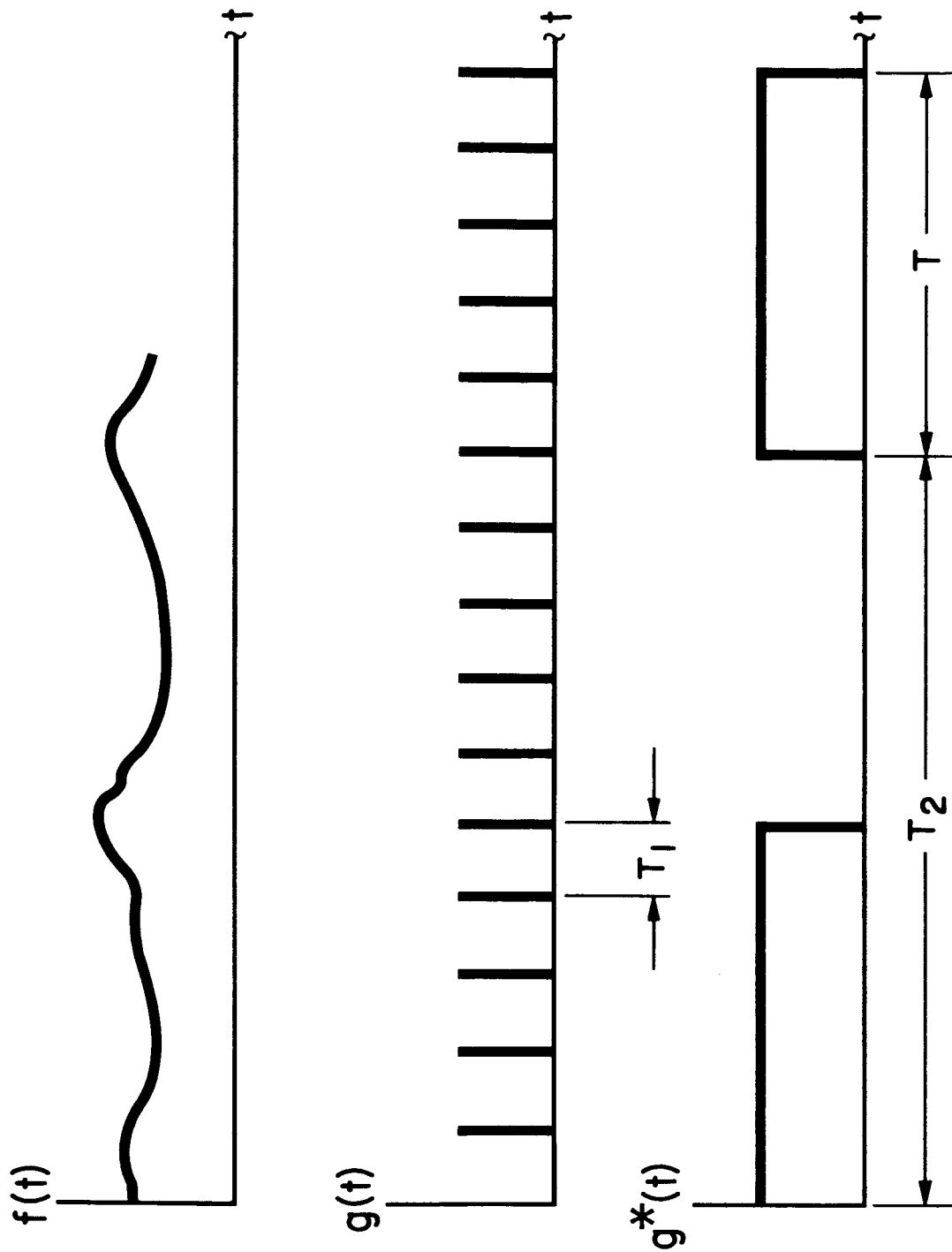
Figure 13.- The signal and switching functions for the general multirate case.
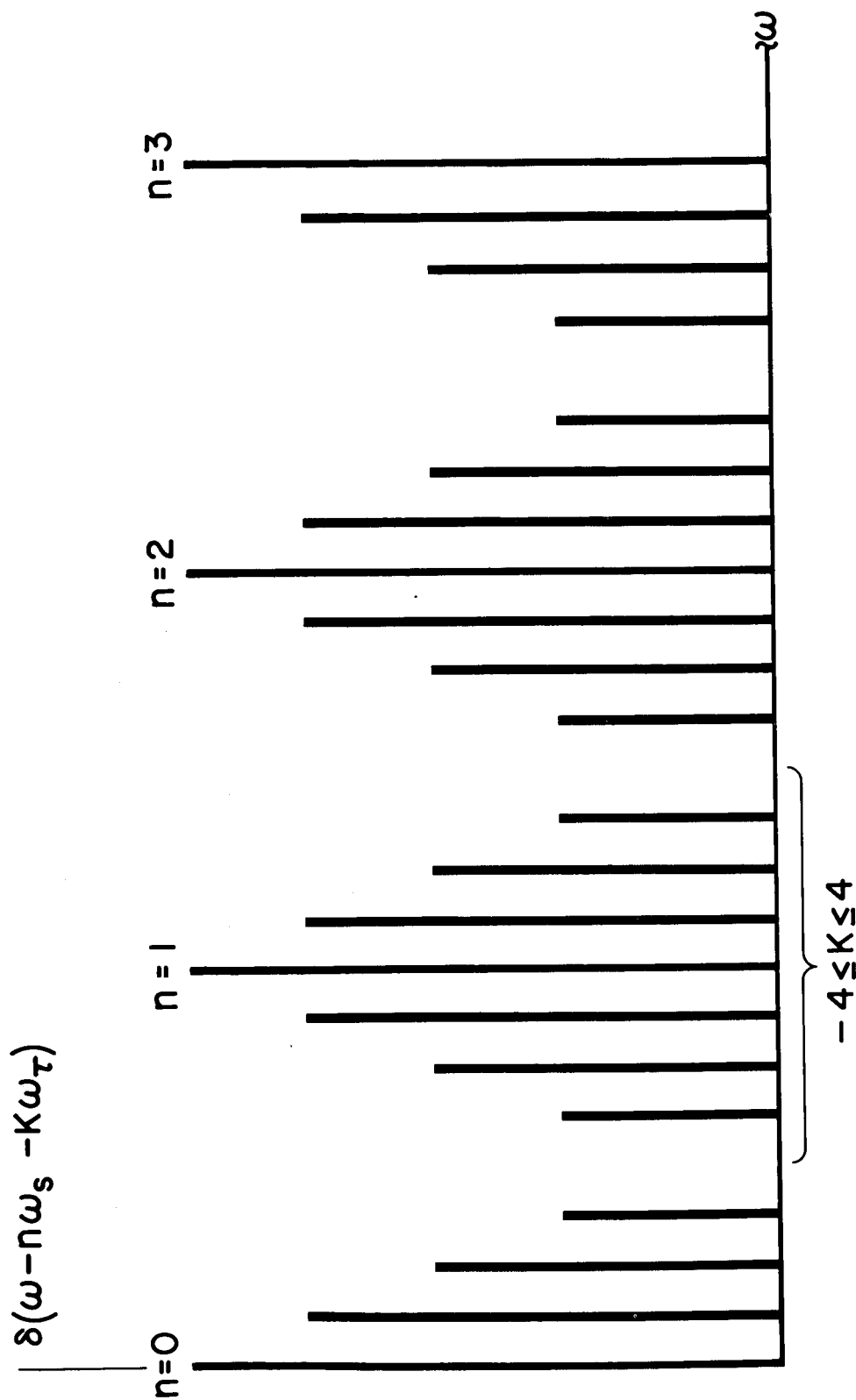
Figure 14.- Multiplet generation showing only the first lobes of $\sin x/x$ for clarity. Actually extended values display phase reversal which affects line amplitude. The case shown is for $\tau/T_2 \sim 0.25$. The negative ω axis is not shown. It is the mirror of the above.
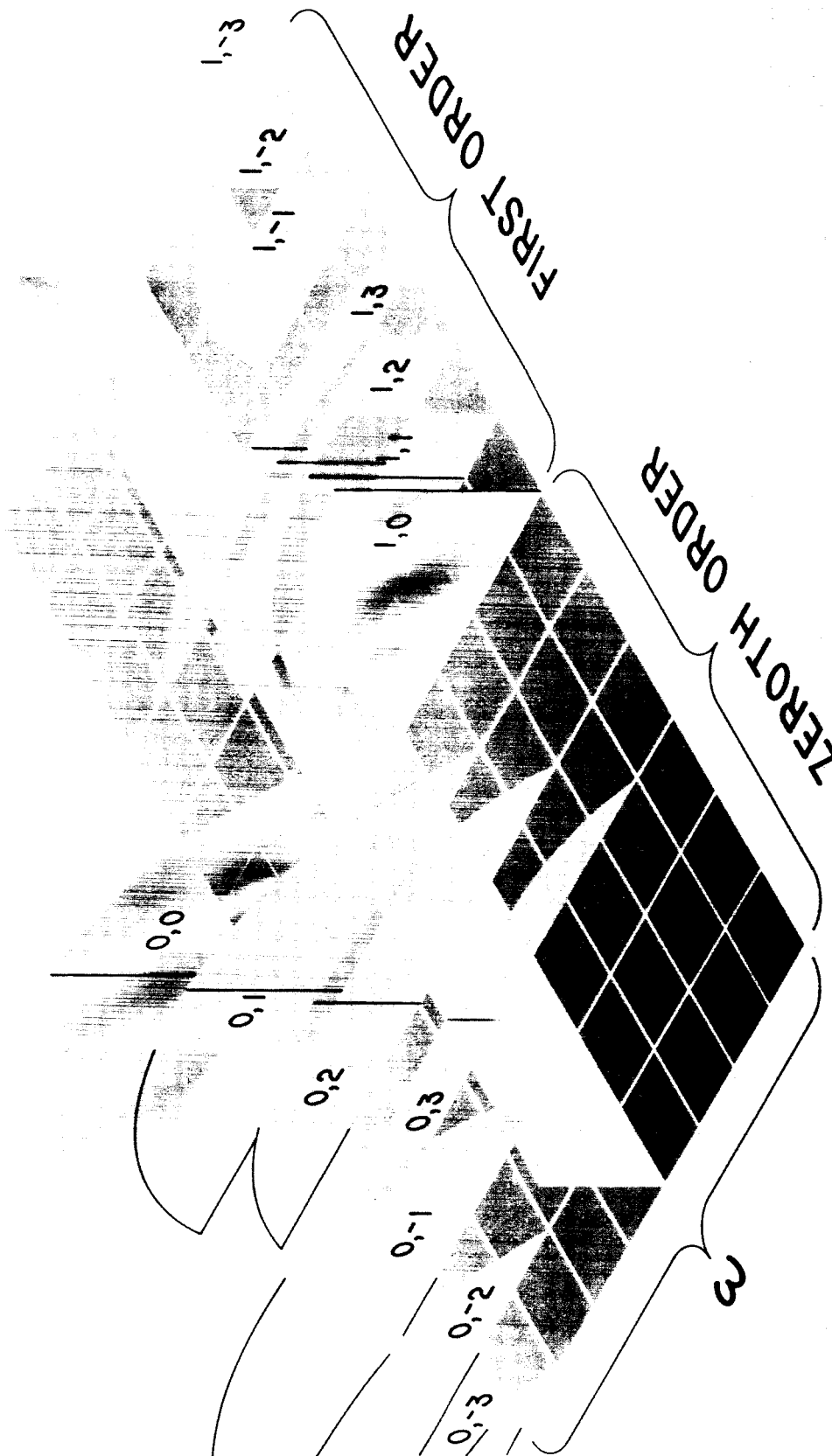
Figure 15.- Reconstruction for a hypothetical data spectrum of the folding configuration for a double periodic sampling function where the ratio of repetition frequencies is T_1/T_2 where T_1 is the periodic sampling interval and T_2 the burst rate. The duty cycle for the burst modulation, $g*(t)$, is 0.25 so that every fourth line is zero. The second-order multiplets for $n = 0$ are not shown. They would lie in the lower figure and be superimposed upon the lines shown. The inversion of the negative frequencies about $n = 0$ are also not shown. The subscripts indicate the order of the spectrum; that is, n, $k = 1$, -3 is the third negative multiplet for $n = 1$.
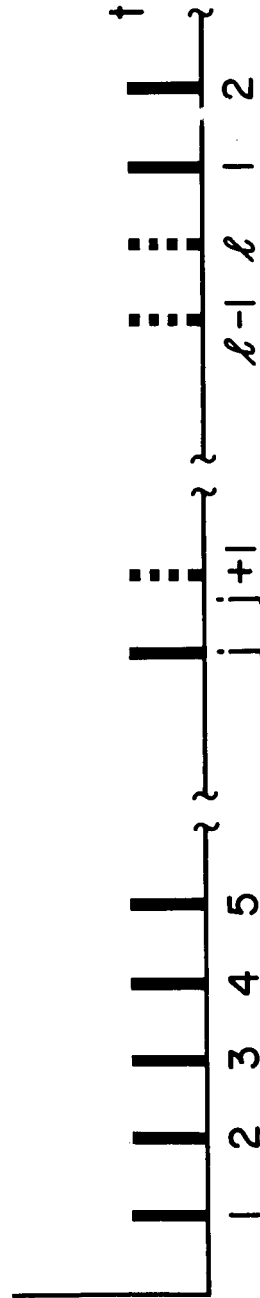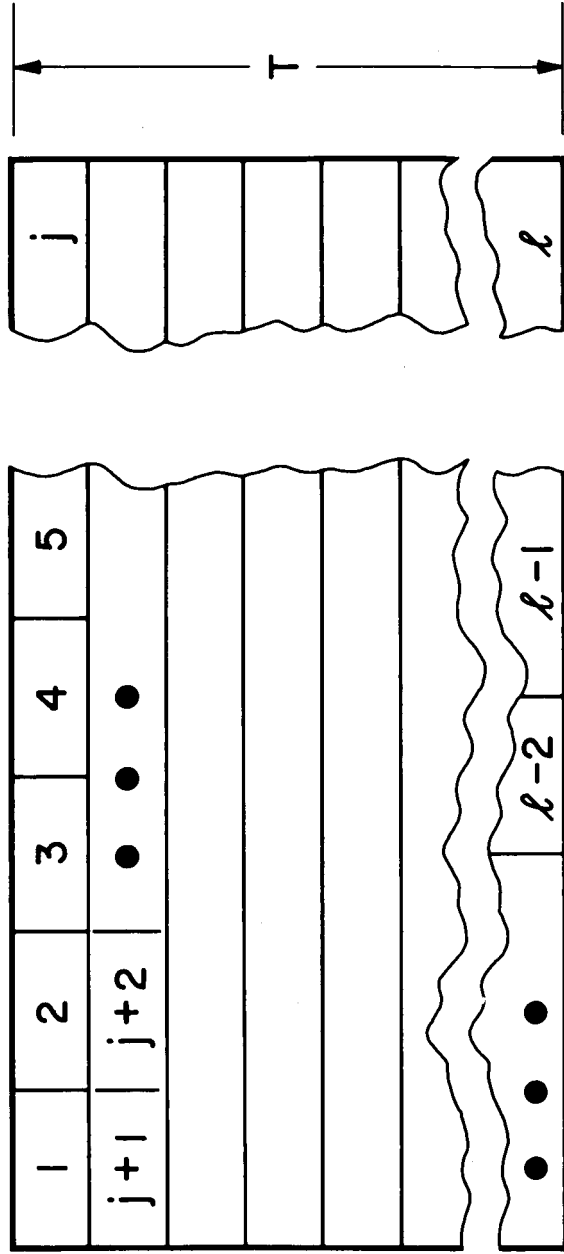
Figure 16.- Format for a standard telemetry distribution as employed in spacecraft showing a hypothetical assignment of j samples followed by l - j blanks. Lower figure shows the time distribution of switching pulses.
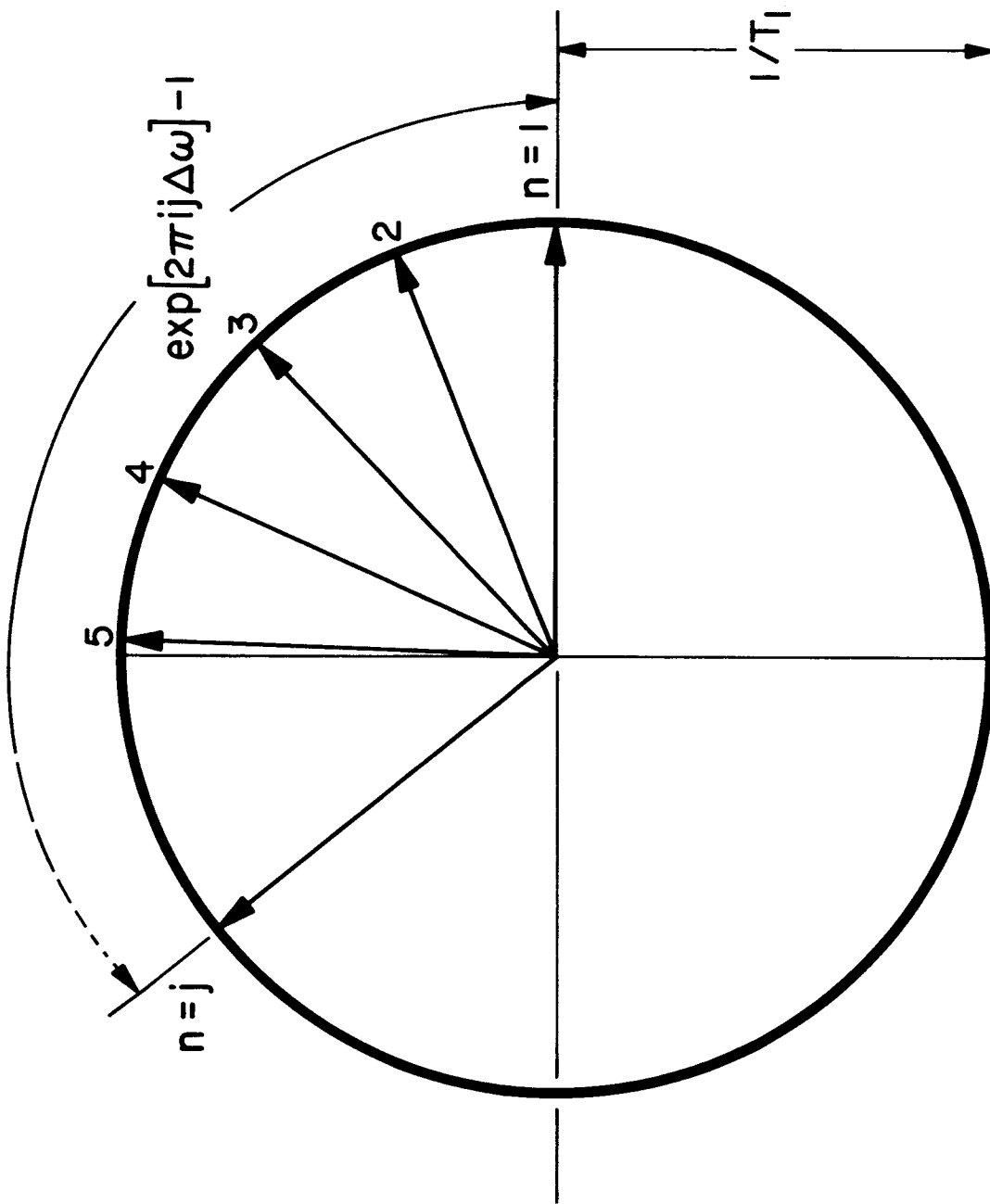
Figure 17.- Vector diagram for the distribution on the circle of radius $1/T_1$ of contributions to the spectral line at the frequency ω. A similar circle is required for each spectral component. As the order of the spectral line is increased, the distribution of vectors expands and becomes modulo 2π.

RELATIVE AMPLITUDE

$\eta = 4/5$

$\eta = 3/5$

$\eta = 2/5$

$\eta = 1/5$

ω_1 ω_2 ω_3 ω_4 ω_5
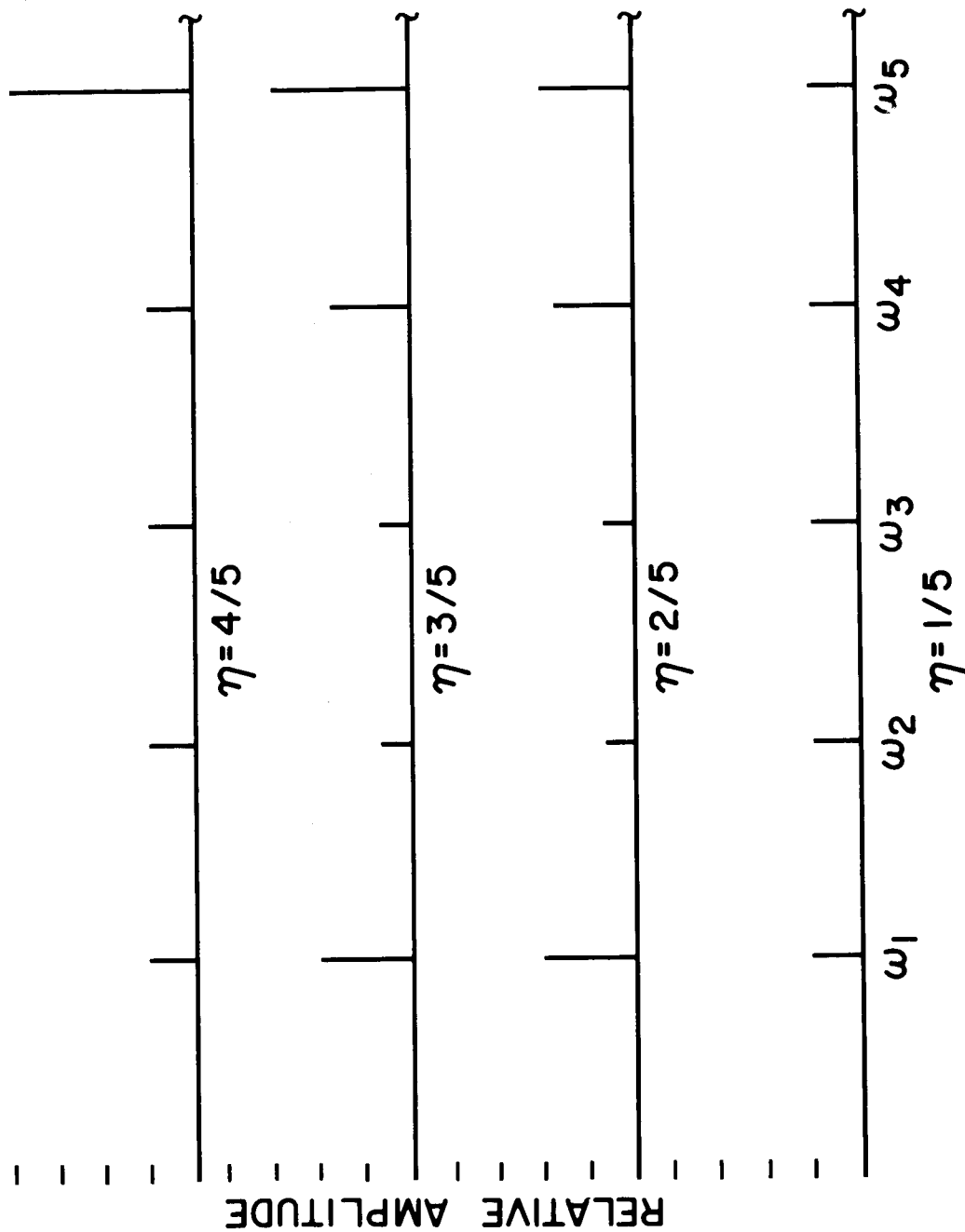
Figure 18.- Spectra of interrupted pulse trains. The top figure represents the case where the original periodicity at $\omega = 5$ has been changed by the removal of every fifth pulse. This causes the introduction of the lower frequency lines. The following cases are for the removal of 2 and 3 pulses and the last is for the removal of 4 out of 5, leaving a basic periodicity 1/5 of the original.
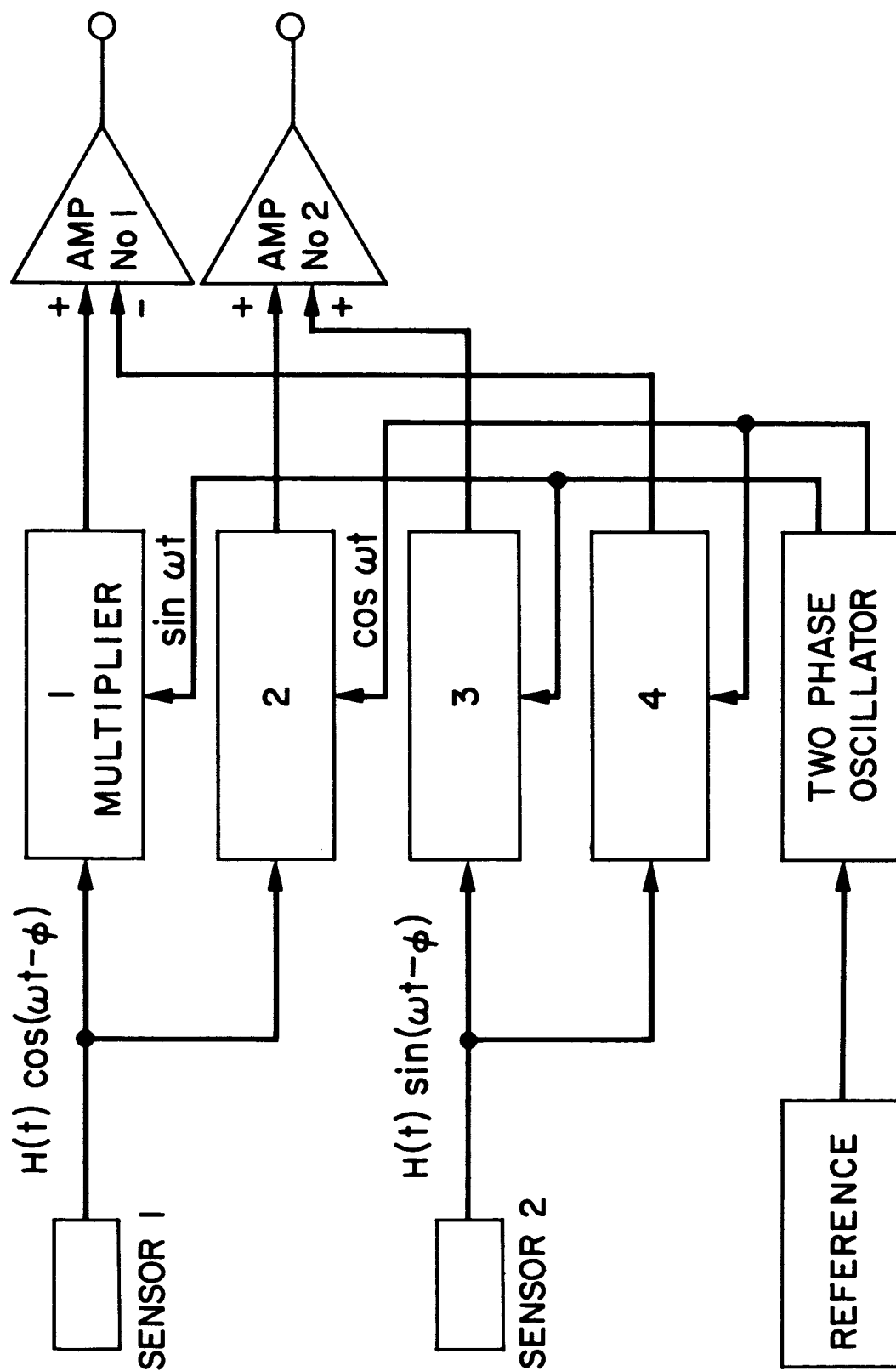
Figure 19.- Simplified block diagram of a spin demodulator system for use with a triaxial flux gate sensor magnetometer. The reference oscillator is driven with a phase locked loop synchronized to the spacecraft sun pulse generator.

A-34441-20

ROTATING SENSOR OUTPUT
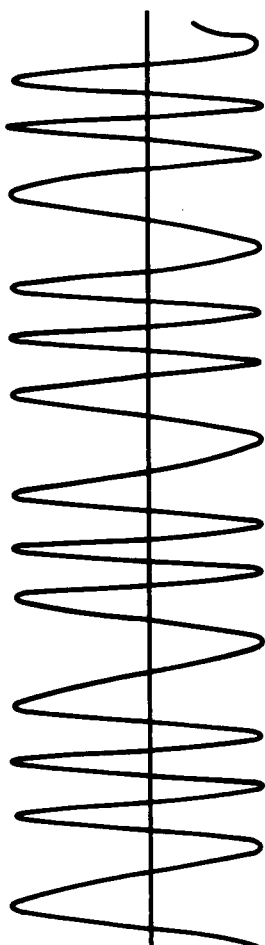
SINE OUTPUT
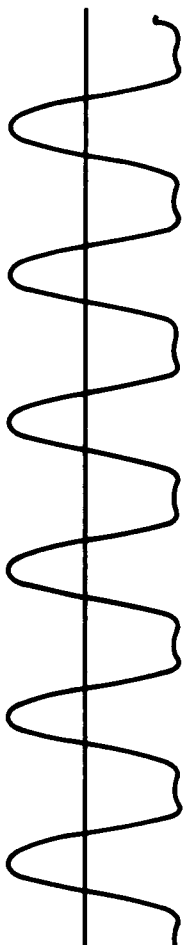
COSINE OUTPUT
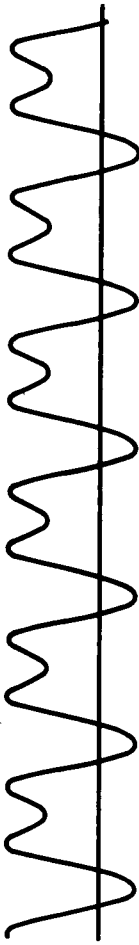
TIME, sec

0   .4   .8   1.2

Figure 20.- Waveforms associated with the simulation of a spinning spacecraft in the presence of an Alfvén wave with an angular excursion of ±π/2. The upper figure shows the waveform generated on one sensor and the lower two waveforms are those from both the sensors mounted in the spin plane of the spacecraft after spin demodulation.

A-34441-21

DEMODULATED
SINE OUTPUT

ω

ω

2ω

DEMODULATED
2ω COSINE OUTPUT

3ω

3ω

4ω

ω/2π, radions/sec

0   0   10   10   20   20   30   30   40   40   50   50
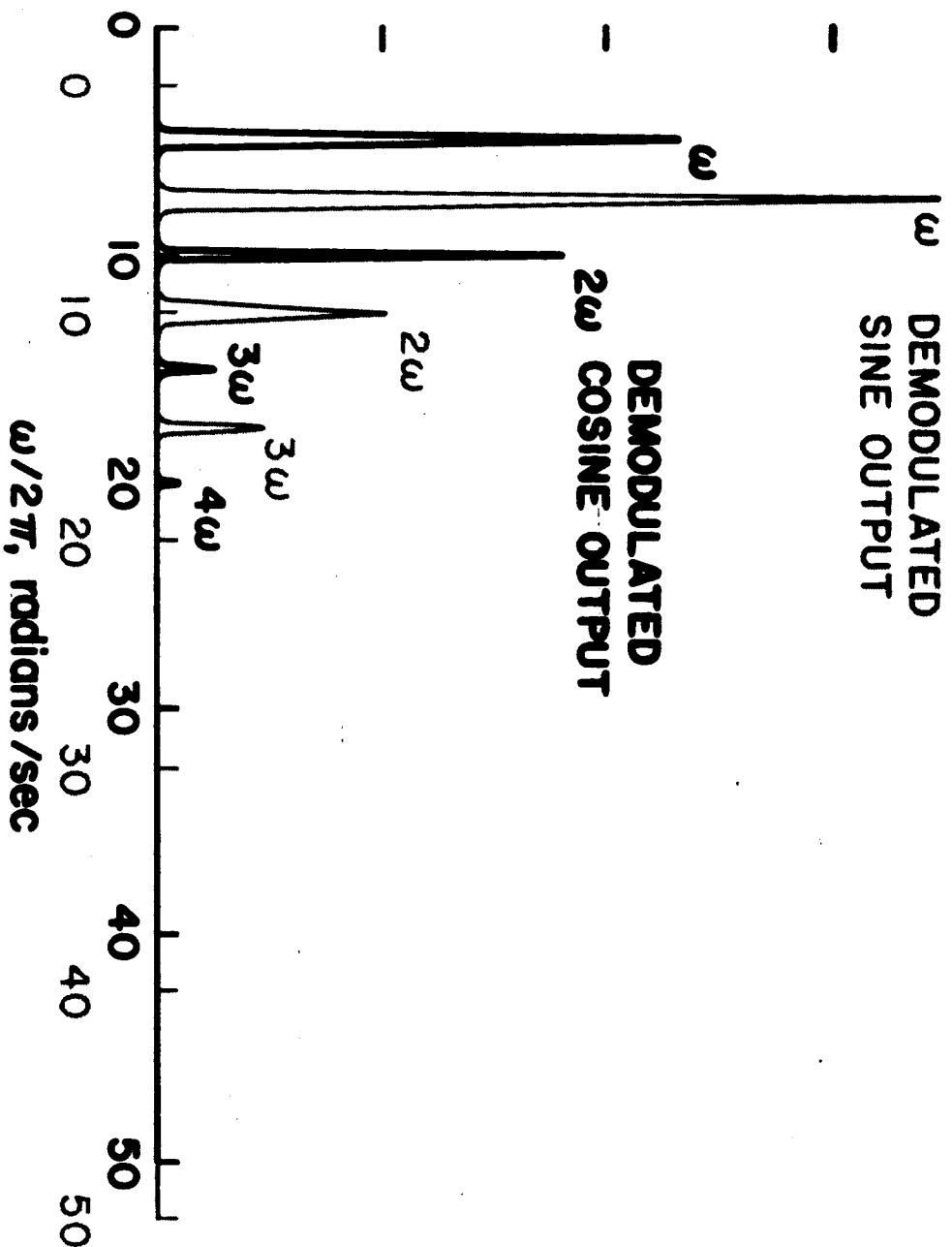
Figure 22.- The demodulated phase spectra associated with both spin plane sensors. The difference in amplitudes is due to the phasing of the plane of the wave as discussed for fig. 21. The amplitudes of the side bands are relative to the unmodulated carrier. Note the folding about zero frequency of the fourth harmonic line on the low frequency end.

A-34441-23

Figure 21.- The spectrum of the Alfvén modulation superimposed upon the spin frequency. The spin frequency is 16 cps and the modulation is 5 cps. This actual spectrum is modified from those shown earlier as follows. The spin frequency is high compared to that of the modulation. Thus the spectrum shown in fig. 8 are folded. Then the effect of the spin is to split the lines as in fig. 9. Both even and odd lines are found for this case due to the assumed orientation of the wave with respect to the sensors.
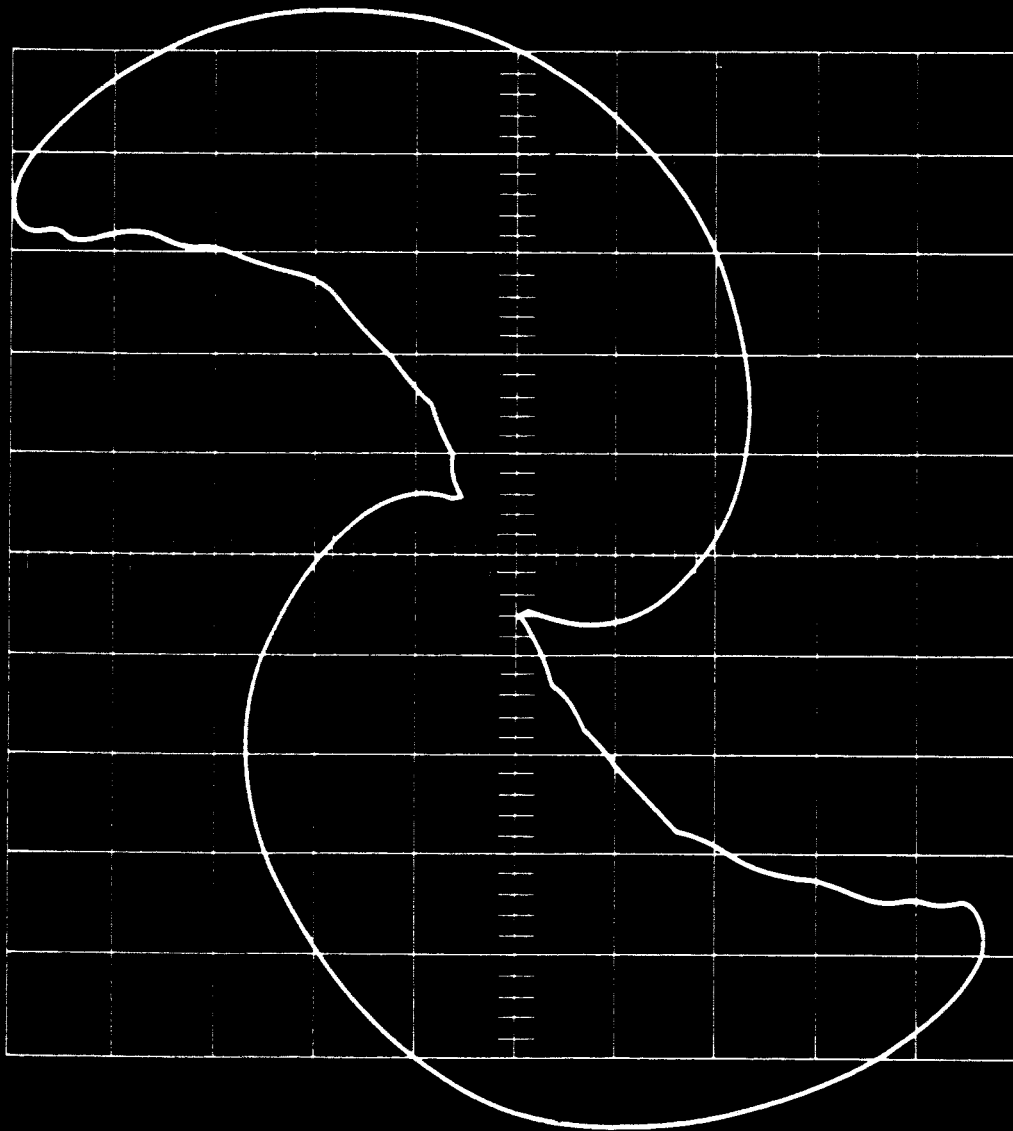
Figure 25.- Waveform of one sensor shown to display the pathological character of the net function.
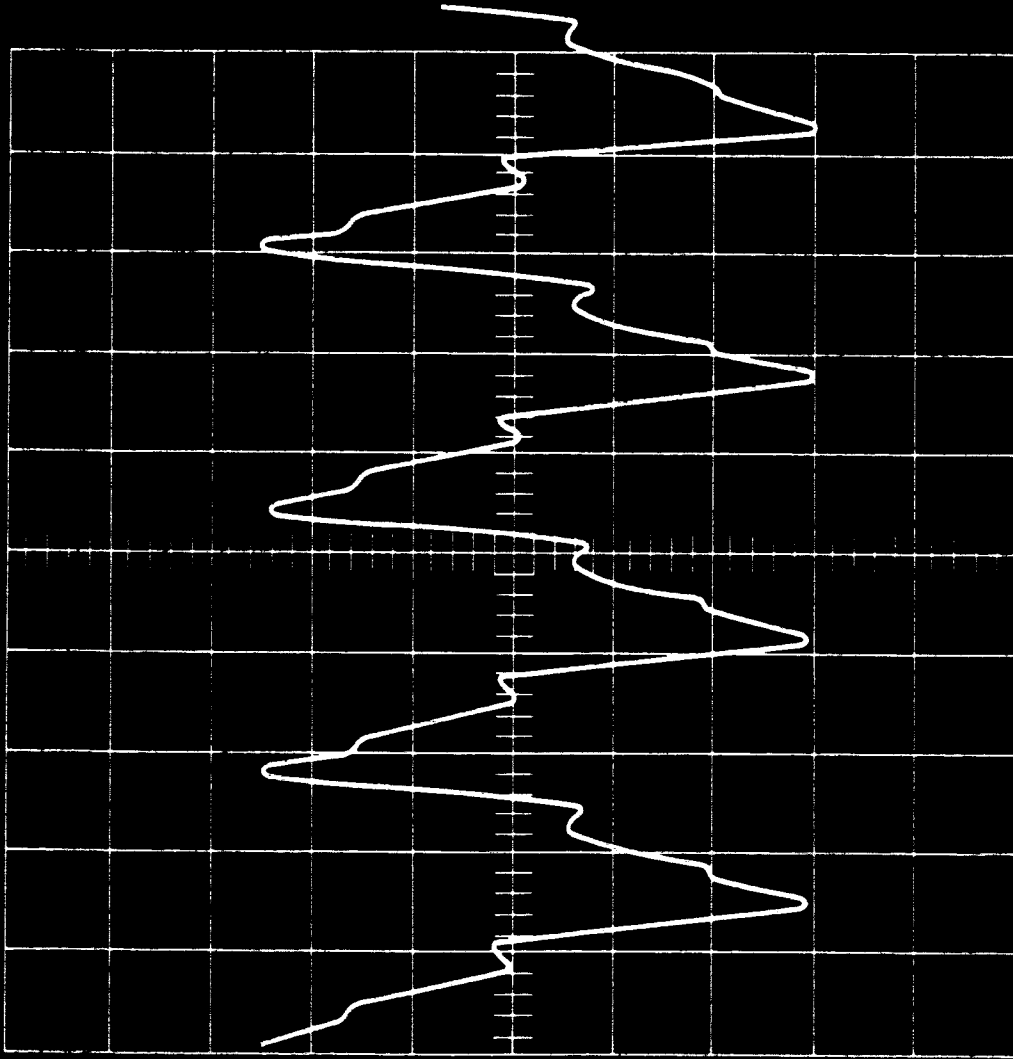
Figure 24.- Lissajou figure of the outputs from two orthogonal sensor simulators for the case of simultaneous Alfvén (vector) and amplitude (scalar) modulation of the base field at twice the spin frequency. The signals shown display the modulation superimposed upon the spin frequency of the spacecraft.
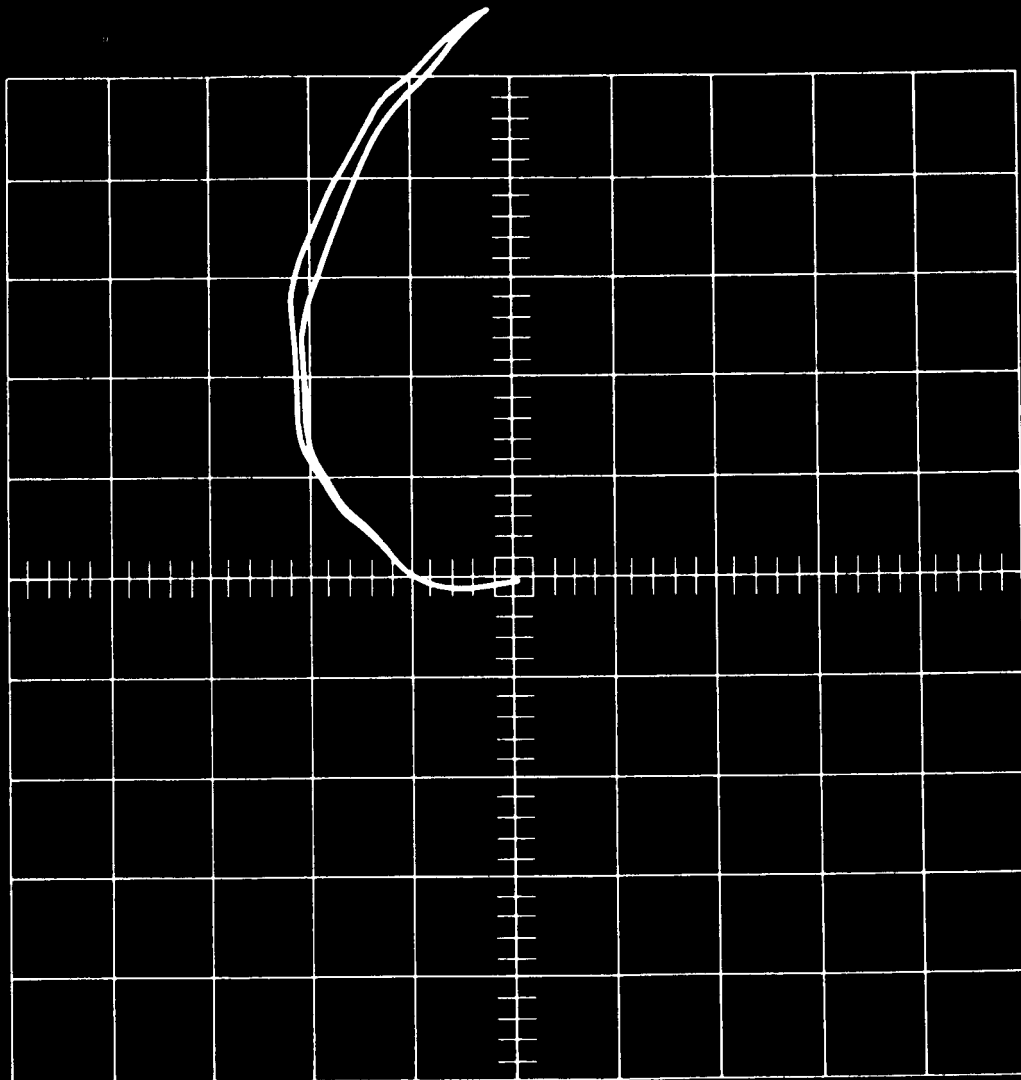
A-34441-26

Figure 23.- x-y plot (Lissajou figure) of the ambient field with vector and scalar modulation as it would appear in space or as measured by a nonrotating spacecraft. This is also the output of the demodulator. The multivalued trace is due to small errors in the function generators.